

CNRS - Université Pierre et Marie Curie - Université Versailles-Saint-Quentin
CEA - ORSTOM - Ecole Normale Supérieure - Ecole Polytechnique

Institut Pierre Simon Laplace

des Sciences de l'Environnement Global

Notes du Pôle de Modélisation

Simulation of the atmospheric sulfur cycle in the Laboratoire de Météorologie Dynamique General Circulation Model. Model Description, Model Evaluation, and Global and European Budgets

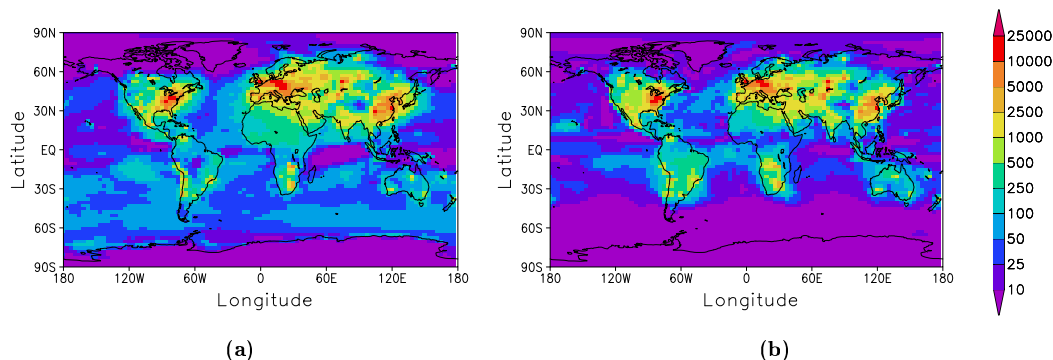
O. Boucher (1), M. Pham (2), C. Venkataraman (3)

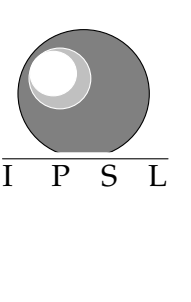
(1) Laboratoire d'Optique Atmosphérique, CNRS / USTL, Villeneuve d'Ascq, France

(2) Service d'Aéronomie, CNRS / UPMC, Paris, France

(3) Centre for Environmental Science and Engineering, Indian Institute of Technology Bombay, India

Distribution of SO_2 mixing ratio (pptv) at the surface in a) January and b) July.



	<p align="center">CNRS - Université Pierre et Marie Curie - Université Versailles-Saint-Quentin CEA - CNES - ORSTOM - Ecole Normale Supérieure - Ecole Polytechnique</p>
	<p align="center">Institut Pierre Simon Laplace des Sciences de l'Environnement Global</p>
	<p align="center">CETP - LMD - LODYC - LPCM - LSCE - SA</p>
<p>Université Pierre-et-Marie-Curie B 102 - T15-E5 - 4, Place Jussieu 75252 Paris Cedex 05 (France) Tél : (33) 01 44 27 39 83 Fax : (33) 01 44 27 37 76</p>	<p align="right">Université Versailles-Saint-Quentin 23 rue du Refuge 78035 Versailles Cedex (France) Tél : (33) 01 39 25 58 23 Fax : (33) 01 39 25 58 18</p>

We have used the Laboratoire de Météorologie Dynamique (LMD) general circulation model to simulate the global sulfur cycle. Processes incorporated in the model include emissions, boundary layer mixing, advective and convective transport, dry and wet scavenging, gaseous- and aqueous-phase chemistry. The model predicts the atmospheric fate of hydrogen peroxide (H_2O_2) and six sulfur species: dimethylsulfide (DMS), dimethylsulfoxide (DMSO), hydrogen sulfide (H_2S), sulfur dioxide (SO_2), sulfate (SO_4^{2-}), and methanesulfonic acid (MSA). The model is evaluated through extensive comparisons to measurements. The model represents many features of the observed concentrations of sulfur species. At remote locations, the agreement with observations is generally good. The surface mixing ratios of sulfur dioxide and sulfate aerosols are underestimated over Europe in winter, and overestimated over North America in summer and autumn. At first order, these discrepancies may be explained by biases in the simulated cloud cover and precipitation fields. A sensitivity run, where H_2O_2 is not depleted upon oxidation of SO_2 , exhibits a large increase in H_2O_2 concentration in wintertime over polluted regions. This indicates that under these conditions this chemical reaction may represent an important sink for H_2O_2 .

<p>Juillet 2002 , Note n° 23</p>

Simulation of the atmospheric sulfur cycle in the Laboratoire de Météorologie Dynamique General Circulation Model. Model Description, Model Evaluation, and Global and European Budgets.

O. Boucher,

Laboratoire d'Optique Atmosphérique, CNRS / USTL, Villeneuve d'Ascq, France

M. Pham

Service d'Aéronomie, CNRS / UPMC, Paris, France

C. Venkataraman

Centre for Environmental Science and Engineering, Indian Institute of Technology Bombay, India

July 4, 2002

Abstract

We have used the Laboratoire de Météorologie Dynamique (LMD) general circulation model to simulate the global sulfur cycle. Processes incorporated in the model include emissions, boundary layer mixing, advective and convective transport, dry and wet scavenging, gaseous- and aqueous-phase chemistry. The model predicts the atmospheric fate of hydrogen peroxide (H_2O_2) and six sulfur species: dimethylsulfide (DMS), dimethylsulfoxide (DMSO), hydrogen sulfide (H_2S), sulfur dioxide (SO_2), sulfate (SO_4^{2-}), and methanesulfonic acid (MSA). The model is evaluated through extensive comparisons to measurements. The model represents many features of the observed concentrations of sulfur species. At remote locations, the agreement with observations is generally good. The surface mixing ratios of sulfur dioxide and sulfate aerosols are underestimated over Europe in winter, and overestimated over North America in summer and autumn. At first order, these discrepancies may be explained by biases in the simulated cloud cover and precipitation fields. A sensitivity run, where H_2O_2 is not depleted upon oxidation of SO_2 , exhibits a large increase in H_2O_2 concentration in wintertime over polluted regions. This indicates that under these conditions this chemical reaction may represent an important sink for H_2O_2 .

1 Introduction

Several sulfur gases are emitted at the Earth's surface from anthropogenic and biogenic activities. Once in the atmosphere, they are transported, oxidized in gas and aqueous phase, and removed by dry and wet deposition. In particular, a large fraction of the gas-phase sulfur dioxide is converted into particulate sulfate. In the seventies, the main concern about the tropospheric sulphur cycle was on the environmental consequences of the man-made sulfur emissions, and particularly the issue of acid rain, since anthropogenic emissions account for more than 60% of the global emissions of sulfur gases (e.g., Rodhe, 1999). In the last ten years, it has been recognized that sulfate aerosols may also affect the climate system (e.g., Charlson et al., 1992). Sulfate aerosols affect the radiation balance, directly through scattering of solar radiation (Boucher and Anderson, 1995), and indirectly by serving as cloud condensation nuclei (CCN), thereby modifying the cloud microphysical and optical properties (Boucher and Lohmann, 1995). Sulfate aerosols also interact chemically with other aerosol types and may play a role in heterogeneous chemistry (Dentener and Crutzen, 1993). In order to assess the

climate forcing due to sulfate aerosols, it is necessary to compute the four-dimensional distribution of sulfate concentration, and thus, to simulate the emissions, transport, and transformation of its precursors.

Although there now exist many model studies on the regional or global sulfur cycle (Langner and Rodhe, 1991; Benkovitz et al., 1994; Pham et al., 1995a, 1995b; Feichter et al., 1996; Chin et al., 1996; Chuang et al., 1997; Kasibhatla et al., 1997; Roelofs et al., 1998; Koch et al., 1999; Adams et al., 1999; Barth et al., 2000; Rasch et al., 2000; Chin et al., 2000a, 2000b), there are still areas of uncertainties. The representation of wet scavenging and aqueous-phase chemistry is generally crude in large-scale models. In particular the relative importances of the different oxidation pathways for SO_2 are not well established. Also many models underpredict wintertime sulfate concentrations over Europe and North-East United States (e.g., Barth et al., 2000; Chuang et al., 2002). The reason for this is uncertain. Some authors believe that there is a missing pathway for SO_2 oxidation in models (Kasibhatla et al., 1997; Roelofs et al., 1998), heterogeneous oxidation

of SO_2 onto aerosols (Kasibhatla et al., 1997) and aqueous-phase oxidation of SO_2 by peroxyntic acid (HNO_4) (Warneck, 1999; Dentener et al., 2002) being some candidates. Chin et al. (2000b) suggested that contamination by sea-salt of the EMEP measurements could partly explain the discrepancy over Europe. Another possibility is that the concentration of one of the oxidants of SO_2 is underestimated in global models. In particular, this could be the case for H_2O_2 if ozonolysis of alkenes – which is usually not considered in global models – turns out to be an important production term for H_2O_2 in wintertime conditions as suggested by Ariya et al. (2000). The discrepancy between observed and simulated sulfate concentrations may also simply be due to deficiencies in the parameterizations of aqueous-phase chemistry and/or wet scavenging, or in the efficiency of the convective transport (Barth et al., 2000).

Here we present a description of the global sulfur cycle as it was introduced in the General Circulation Model (GCM) of the Laboratoire de Météorologie Dynamique (LMD-ZT). The model is thoroughly evaluated against available measurements. The budgets of sulfur species and H_2O_2 – and their coupling to each other – are discussed. We favored an on-line, in contrast to off-line, approach because we are interested in studying climate-chemistry interactions. By doing so, it is possible to represent to a high degree of consistency the physical and chemical processes of the sulfur cycle. However it is clear that inaccuracies in the simulation of the hydrological cycle (e.g., cloudiness, precipitation) can result in significant biases in the simulated concentrations of the sulfur species. LMD-ZT can also be nudged to meteorological analyses so that comparison with observations at a specific place and time is possible (Hourdin and Issartel, 2000). In the simulations presented in this study, the radiative impact of sulfate aerosols does not feedback on the meteorology. Work is in progress to include a full interactive gas-phase chemistry, as well as carbonaceous, sea-salt, and dust aerosols in the same version of the model. We will then have a useful tool to study the chemical interactions among the different aerosol species. The model will also be used to compute the aerosol radiative forcing and to run scenarios

of climate change with the forcings from greenhouse gases and aerosols included.

2 Description of the Model

2.1 LMD-ZT

In LMD-ZT, atmospheric transport is computed with a finite volume transport scheme for large-scale advection (van Leer, 1977; Hourdin and Armangaud, 1999), a scheme for turbulent mixing in the boundary layer, and a mass flux scheme for convection (Tiedtke, 1989). The resolution is 3.75° in longitude, 2.5° in latitude (corresponding roughly to the resolution of a T48 spectral model, Hourdin, personal communication) and 19 layers on the vertical. In this version (referred to as 3.3), a hybrid σ -pressure coordinate on the vertical is used, with 5 layers below about 850 hPa and 9 layers above about 250 hPa. The time step is 3 min for resolving the dynamical part of the primitive equations. Mass fluxes are cumulated over 5 time steps so that large-scale advection is applied every 15 min. The physical and chemical parametrizations are applied every 10 time steps or 30 min. The different processes are handled through operator splitting.

In its present version, the model exhibits a too low precipitation rate and cloud cover over continental areas in summertime, and a too large precipitation rate and cloud cover over Europe in wintertime. The precipitation field is shown on Fig. 1 in annual mean along with observations from Legates and Willmott (1990).

Six sulfur species are considered in the model: dimethylsulfide (DMS), dimethylsulfoxide (DMSO), hydrogen sulfide (H_2S), sulfur dioxide (SO_2), sulfate (SO_4^{2-}), and methanesulfonic acid (MSA). Sulfate and MSA are assumed to be 100% in the particulate phase. The concentrations of short-lived radicals OH, HO_2 , and NO_3 , and ozone, as well as H_2O_2 photodissociation rates, are prescribed from version 3.2 of the Intermediate Model of Global Evolution of Species (IMAGES) (Müller and Brasseur, 1995). The diurnal cycles of these fields are

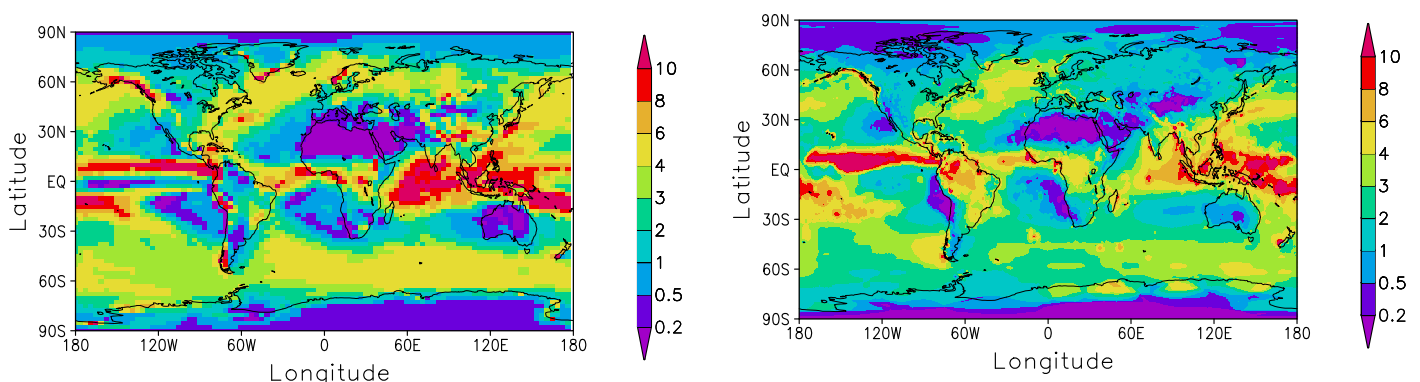


Fig. 1: Annual-mean precipitation rate (mm/day) in LMD-ZT (left panel) and the Legates and Willmott (1990) climatology (right panel).

archived from IMAGES for each month and applied in our model with a time step of 30 minutes, which is also the time step for the physical and chemical processes. Because the concentration of hydrogen peroxide H_2O_2 can be significantly affected upon oxidation of SO_2 , especially at high latitude in wintertime, it is also a prognostic variable of the model. Its concentration is computed from prescribed OH and HO_2 concentrations and H_2O_2 photodissociation rates archived from IMAGES. It also undergoes dry and wet scavenging and advective and convective transport.

2.2 Emissions

Emissions of sulfur species are summarized in Table 1. SO_2 is emitted primarily by anthropogenic activities. Here we make use of the emission inventory developed in the framework of the Global Emissions Inventory Activity (GEIA). Our annual emission rate ($66.3 \text{ Tg S yr}^{-1}$), representative of the year 1985, is close to the emission rates of Koch et al. (1999) and Barth et al. (2000) but lower than that of Chin et al. (2000a). A small fraction (5%) of SO_2 is emitted directly as sulfate (Benkovitz et al., 1996). We include an anthropogenic source of H_2S of $2.82 \text{ Tg S yr}^{-1}$ scaled to the SO_2 source, following the estimate of Watts (2000).

Table 1: Globally- and annually-averaged emission fluxes of sulfur species (Tg S yr^{-1}).

Sources	SO_2	H_2S	DMS	Total
Volcanoes	4.81			4.81
Biosphere		0.51	0.31	0.82
- Vegetation		0.49	0.29	
- Soils		0.02	0.02	
Biomass burning	2.99			2.99
Ocean			19.10	19.10
Man-made	66.28	2.82		69.10
Total	74.08	3.33	19.41	96.82

5% of the man-made SO_2 is emitted directly as sulfate.

We only consider volcanic sources of SO_2 from continuously erupting volcanoes, which represents an emission rate of 4.8 Tg S yr^{-1} (Andres and Kasgnoc, 1998).

Biogenic emissions are dominated by the oceanic emission of DMS, the flux of which is derived off-line from the sea surface DMS concentrations of Kettle et al. (1999) and the sea to air parameterization of Liss and Merlivat (1986). The seasonal cycle in DMS emission is very pronounced, especially at $40\text{--}50^\circ\text{S}$. At $19.4 \text{ Tg S yr}^{-1}$, our total emission rate for DMS is significantly larger than those of Koch et al. (1999), Barth et al. (2000), and Chin et al. (2000a), which are 10.7, 15.5, and $13.3 \text{ Tg S yr}^{-1}$, respectively, and were obtained using different methodologies or DMS concentration fields. It is nevertheless in the middle of the range of 10 to 40 Tg S yr^{-1} usually accepted for DMS emissions. We are currently studying the sensitivity of on-line computation of the DMS emission flux to oceanic DMS concentration and air-sea flux parametrization (Cosme et al., 2002; Boucher et al., 2002). Emissions of DMS and H_2S from the biosphere and emissions of SO_2

from biomass burning are the same as in the IMAGES model (Pham et al., 1995a). They are much smaller compared to the other sources of sulfur compounds (i.e., DMS from the ocean and man-made SO_2 , see Table 1).

2.3 Gas-Phase Chemistry

Gas-phase chemistry is based on the scheme introduced in Pham et al. (1995a). The reactions and reaction rates are tabulated in Table 2. DMS is oxidized by OH and NO_3 radicals producing SO_2 and DMSO. No other reaction was considered for DMS, in contrast to Chin et al. (1996) who assumed the presence of an additional oxidant to increase the oxidation rate of DMS by a factor of 2. Following Chatfield and Crutzen (1990), we assume that MSA production proceeds via DMSO through the addition pathway of DMS oxidation. This should be investigated in future studies according to Sciare et al. (1998), who suggested that MSA and DMSO production proceeds through two different channels, namely the abstraction and addition channels respectively. H_2S is oxidized by OH but contributes to a very small fraction of the total production rate of SO_2 . The distribution of H_2S and DMSO will not be discussed further because of their small burdens and large uncertainties, but their contributions to the global sulfur budget are included for completeness.

Gas-phase H_2O_2 is formed primarily through the reaction of HO_2 given in Table 2, which includes a bimolecular component, a termolecular component, and an enhancement component due to water vapor. This enhancement is about a factor of 2.6 at 100% relative humidity and 298 K. H_2O_2 is removed from the atmosphere by dry and wet deposition (see Section 2.5), by the gas-phase processes of solar photolysis and reaction with the OH radical, and upon the aqueous-phase oxidation of SO_2 (see below). The diurnal variation in H_2O_2 concentration is therefore simulated consistently with the concentrations of OH and HO_2 and H_2O_2 photodissociation rates.

The gas-phase reactions are evaluated using a 30-min time step with an explicit scheme. This scheme can be used because of the long lifetimes of all of the prognostic chemical species considered here. Moreover it makes easy to compute a mass-balanced sulfur budget (cf. Section 7).

2.4 Aqueous-Phase Chemistry

Aqueous-phase oxidation of SO_2 by O_3 and H_2O_2 is also considered. The concentration of O_3 is prescribed using the results from the IMAGES model, but that of H_2O_2 is computed interactively. The cloud pH is predicted by an electroneutrality equation in which NH_4^+ and H^+ are the only cations and NO_3^- is neglected, as follows:

$$[\text{H}^+] = 2 [\text{SO}_4^{2-}] + 2 [\text{SO}_3^{2-}] + [\text{HSO}_3^-] + [\text{OH}^-] - [\text{NH}_4^+] \quad (1)$$

From global sulphate concentrations summarised by Seinfeld and Pandis (1998) and measurements by Covert (1988), a cloudwater $[\text{NH}_4^+]/[\text{SO}_4^{2-}]$ molar ratio of 1.0 is

assumed in remote environments and of 1.5 in polluted environments, where cloudwater sulphate concentrations exceeds 15 μM .

Aqueous S_{IV} species are estimated accounting for ionisation of $\text{SO}_2\text{-H}_2\text{O}$ using the first and second dissociation constants (Table 2). It is assumed that in-cloud oxidation is not limited by mass transfer (Venkataraman et al., 2001) and would depend only on the gas-phase concentrations of SO_2 and the oxidants. Aqueous S_{IV} species are oxidised by ozone and hydrogen peroxide which partition into aqueous phase following Henry’s law (Table 2). Dentener et al. (2002) showed that aqueous-phase oxidation of HSO_3^- by HOONO_2 could contribute to sulfate formation. However, this reaction has also been shown to significantly alter H_2O_2 and O_3 concentrations in the boundary layer (Dentener et al., 2002). Since this pathway is still uncertain and O_3 is not simulated by the gas-phase chemistry scheme adopted here, we chose to ignore this reaction in the present study.

The rate expressions and rate constants for the aqueous phase reactions (Table 2) are summarised by Seinfeld and Pandis (1998) based on a best fit to the available kinetic data from various studies (Hoffmann and Calvert, 1985).

Because the reaction rate of aqueous O_3 with SO_2 is pH-dependent (see Table 2), the 30 min time step is split into 15 time steps of 2 min each, for which the oxidation reaction rates and the cloud pH are computed. Aqueous-phase SO_2 oxidation only occurs in the cloudy part of the grid-box; we do not allow mixing of air between clear and cloudy sky during the 30 min time step (i.e., if SO_2 or H_2O_2 are completely consumed in the cloud part of the grid-box, we do not allow SO_2 or H_2O_2 from the clear part to be also consumed). We assume a linear transition between ice and liquid clouds in the temperature range of -20° to -10°C . The fraction of condensate that is liquid in the cloud varies from 1 at -10°C to 0 at -20° . No “aqueous-phase” chemistry takes place in ice clouds. Therefore aqueous-phase chemistry is completely shut off below -20°C . No aqueous-phase chemistry is considered in rain or snow.

2.5 Dry and Wet Deposition

Dry deposition is parameterized through deposition velocities, which are prescribed for each chemical species and surface type (Table 3). A more appropriate formulation which depends on vegetation type and atmospheric stability is under development.

Wet deposition (or scavenging) is treated separately

for stratiform and convective rain. For in-cloud scavenging, we apply a parameterization similar to that of Giorgi and Chameides (1986). The scavenging rate (s^{-1}) is given by

$$W = \beta f r \quad (2)$$

where f is the cloud volume fraction, r the fraction of the chemical species that is in the aqueous phase, and β is the rate of conversion of cloudwater to rainwater (in unit of $\text{kg kg}^{-1} \text{s}^{-1}$). The parameter r is obtained assuming Henry’s law equilibrium for gases and is set to 0.7 for sulfate and MSA aerosols. This reflects the fact that a fraction of sulfate aerosols can be interstitial in clouds as shown by a number of measurements (Boucher and Lohmann, 1995). The parameter β at model level k is computed from the three-dimensional precipitation flux (P_r , stratiform or convective, in $\text{kg m}^{-2} \text{s}^{-1}$) and a prescribed liquid water content ($q_l=0.5$ and 1.0 g kg^{-1} for stratiform and convective clouds, respectively):

$$\beta_k = \frac{P_{r,k} - P_{r,k+1}}{\rho_{\text{air},k} \Delta z_k f_k q_l} \quad (3)$$

where ρ_{air} is the air density (kg m^{-3}) and Δz_k is the thickness of layer k . We do not distinguish between liquid and ice precipitation as far as in-cloud scavenging is concerned.

Below-cloud scavenging is considered for aerosols only. By integrating over the population of raindrops the volume of space that is swept by a raindrop during its fallout, the expression for the scavenging rate (s^{-1}) is:

$$K = \frac{3 P_r \alpha}{4 R_r \rho_{\text{water}}} \quad (4)$$

where R_r is an average raindrop radius (set to 1 mm here), ρ_{water} the water density (kg m^{-3}), and α is the efficiency with which aerosols are collected by raindrops. For the parameter α , we selected a value of 0.001 and 0.01 for raindrops and snowflakes, respectively, based on measurements compiled by Pruppacher and Klett (1997).

Because the three-dimensional precipitation fluxes are available in the GCM, we do not have to assume an ad-hoc vertical profile of precipitation. and EMEFS, respectively. Model results are also compared to surface of raindrops. The release at a level k is equal to the amount of the given species which was scavenged at higher levels multiplied by the fraction of precipitation which is evaporated. For aerosols, a multiplicative factor of 0.5 is applied to account for the fact that raindrops can shrink without evaporating totally. In the event of a total evaporation of the precipitation flux, the aerosols are released totally as well.

Table 2: Reaction rates used in the present study.

Reaction	Rate	Reference
<i>Gaseous-Phase Chemistry</i>		
DMS + OH \rightarrow SO ₂ + ...	$K_1 = 9.6 \cdot 10^{-12} e^{-234./T}$	a
DMS + OH $\rightarrow x\text{SO}_2 + (1-x)\text{DMSO} + \dots$	$\begin{cases} K_2 = 3.04 \cdot 10^{-12} e^{350./T} \alpha / (1 + \alpha) \\ \alpha = 1.15 \cdot 10^{-31} e^{7460./T} [M] & x = 0.6 \end{cases}$	b
DMS + NO ₃ \rightarrow SO ₂ + ...	$K_3 = 1.9 \cdot 10^{-13} e^{500./T}$	c
SO ₂ + OH \rightarrow sulfate + ...	$\begin{cases} K_4 = \alpha [M] / (1 + \alpha [M]) / 1.5 \cdot 10^{-12} \cdot 0.6^\beta \\ \alpha = 3.0 \cdot 10^{-31} (300./T)^{3.3} \\ \beta = 1. / (1 + \log_{10}(\alpha [M] / 1.5 \cdot 10^{-12}))^2 \end{cases}$	c
DMSO + OH $\rightarrow x\text{SO}_2 + (1-x)\text{MSA} + \dots$	$K_5 = 5.8 \cdot 10^{-11} \quad x = 0.6$	b
H ₂ S + OH \rightarrow SO ₂ + ...	$K_6 = 6.0 \cdot 10^{-12} e^{-75./T}$	c
HO ₂ + HO ₂ \rightarrow H ₂ O ₂ + ...	$\begin{cases} K_7 = 2.3 \cdot 10^{-13} e^{600./T} + 1.7 \cdot 10^{-33} [M] e^{1000./T} \\ \text{corrected for the effect of water vapour} \end{cases}$	c
H ₂ O ₂ + OH \rightarrow HO ₂ + H ₂ O	$K_8 = 2.9 \cdot 10^{-12} e^{-160./T}$	c
H ₂ O ₂ + h ν \rightarrow 2 OH	Prescribed from IMAGES	
<i>Aqueous-Phase Chemistry</i>		
S(IV) + H ₂ O ₂ \rightarrow sulfate	$K_{11}^{\text{aq}} = 7.5 \cdot 10^7 e^{-4430(1/T-1/298.)} [H^+]_{\text{aq}} / (1 + 13[H^+]_{\text{aq}})$	d
S(IV) + O ₃ \rightarrow sulfate	$\begin{cases} K_{21}^{\text{aq}} = 2.4 \cdot 10^4 \\ K_{22}^{\text{aq}} = 3.7 \cdot 10^5 e^{-5530(1/T-1/298.)} \\ K_{23}^{\text{aq}} = 1.5 \cdot 10^9 e^{-5280(1/T-1/298.)} \end{cases}$	d
<i>Solubility Constants</i>		
DMSO	$5 \cdot 10^4$	e
SO ₂	$1.4 e^{2900(1/T-1/298.)}$	f
H ₂ O ₂	$8.3 \cdot 10^4 e^{7400(1/T-1/298.)}$	g
O ₃	$1.15 \cdot 10^{-2} e^{2560(1/T-1/298.)}$	h
<i>Dissociation Constants</i>		
SO ₂ / SO ₃ ⁻	$1.3 \cdot 10^{-2} e^{1960(1/T-1/298.)}$	d
SO ₃ ⁻ / SO ₃ ²⁻	$6.6 \cdot 10^{-8} e^{1500(1/T-1/298.)}$	d

Units are cm³ molec⁻¹ s⁻¹ for the gas-phase reaction rates (K_i), l mol⁻¹ s⁻¹ for aqueous-phase reaction rates

(K_{ij}^{aq}), mol l atm⁻¹ for solubility constants, and mol l⁻¹ for dissociation constants.

a Atkinson et al. (1989), b Chatfield and Crutzen (1990), c DeMore et al. (1997), d Seinfeld and Pandis (1998)

e Sander (1999), f Lide and Frederikse (1995), g O'Sullivan et al. (1996), h National Bureau of Standards (1965).

$$\frac{\partial [\text{S}_{\text{iv}}]_{\text{aq}}}{\partial t} = -K_{11}^{\text{aq}} [\text{H}_2\text{O}_2]_{\text{aq}} [\text{HSO}_3^-]_{\text{aq}} \quad \frac{\partial [\text{S}_{\text{iv}}]_{\text{aq}}}{\partial t} = -(K_{21}^{\text{aq}} [\text{SO}_2 \cdot \text{H}_2\text{O}]_{\text{aq}} + K_{22}^{\text{aq}} [\text{HSO}_3^-]_{\text{aq}} + K_{23}^{\text{aq}} [\text{SO}_3^{2-}]_{\text{aq}}) [\text{O}_3]_{\text{aq}}$$

Table 3: Dry deposition velocities (cm s⁻¹).

	DMS	SO ₂	H ₂ S	DMSO ^c
Ocean	0.0	0.7 ^a	0.0	1.0
Land	0.0	0.2 ^b	0.0	0.0
Ice	0.0	0.2	0.0	0.0
	MSA ^d	Sulfate ^d	H ₂ O ₂	
Ocean	0.05	0.05	1.0	
Land	0.25	0.25	1.5	
Ice	0.25	0.25	0.04	

a Garland (1977)

b Clarke et al. (1997)

c Chatfield and Crutzen (1990)

d Wesely et al. (1985)

2.6 Convective Transport

We use the mass fluxes simulated by the Tiedtke (1989) scheme to parameterize convective transport of gases and aerosols. We account for the vertical transport of trace species in updrafts, downdrafts, and in the environment, and for entrainment and detrainment from and to the environment. The convective transport is performed after

the wet scavenging calculation in order to avoid upwards transport of material which is necessarily scavenged by precipitation. In addition, we scavenge a fraction of the soluble tracers released to the environment (Balkanski et al., 1993; Mari et al., 2000; Crutzen and Lawrence, 2000). This fraction is set to 20% and 50% for gases (except DMS) and aerosols, respectively. Note that we apply convective transport in a bulk manner without distinguishing between the interstitial and the dissolved fractions of trace gases and aerosols. This is in contrast with Barth et al. (2000) who treat separately interstitial and dissolved material.

3 Results

Our model is run for 18 months. In the following sections, surface and zonal distributions as well as comparisons with observations are presented for the results of the last 12 months.

There are numerous measurements of DMS, SO₂, sulfates, and MSA from campaigns or continuously monitor-

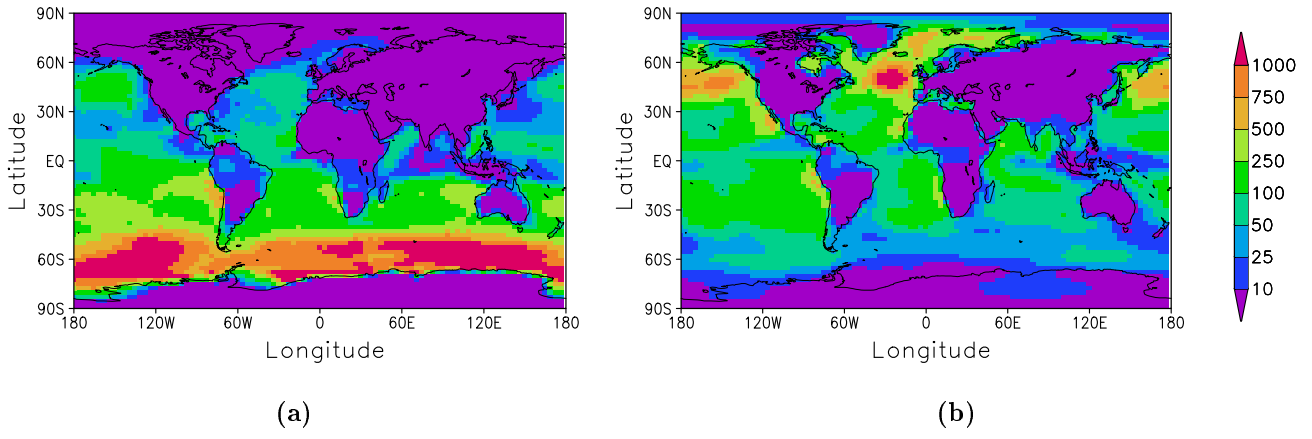


Fig. 2: Distribution of DMS mixing ratio (pptv) at the surface in a) January and b) July.

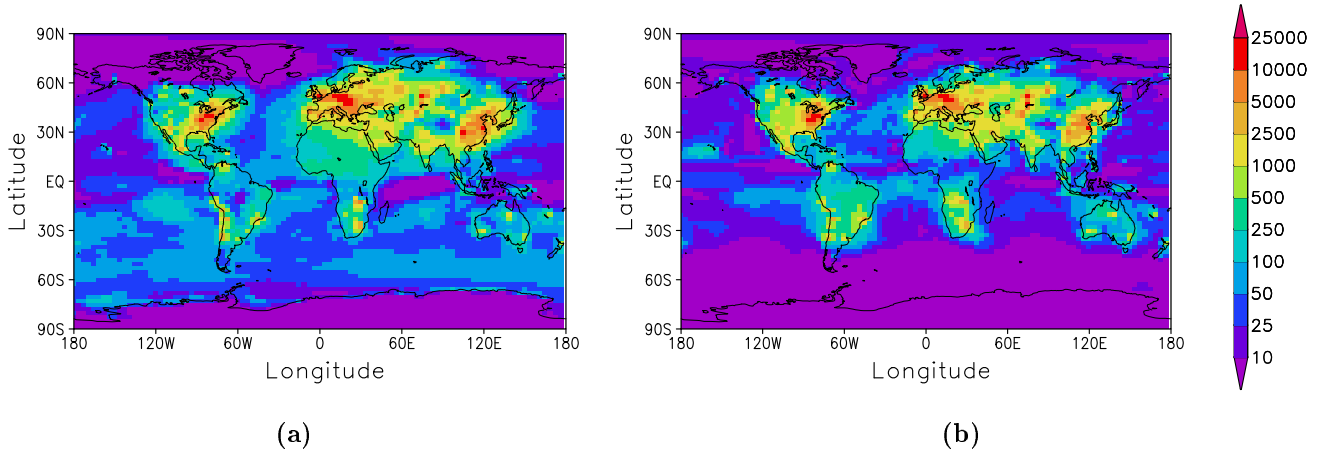


Fig. 3: Distribution of SO_2 mixing ratio (pptv) at the surface in a) January and b) July.

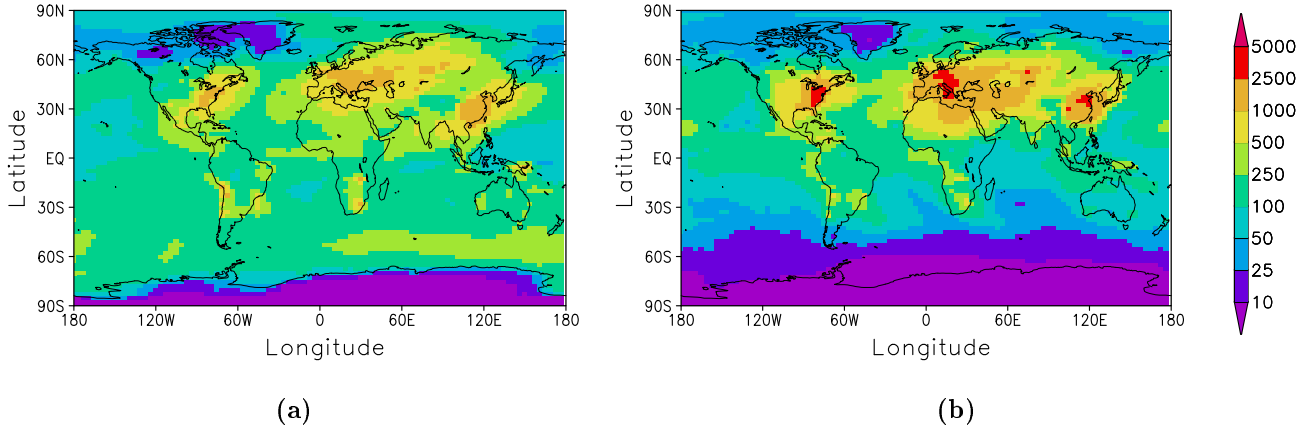


Fig. 4: Distribution of sulfate mixing ratio (pptv) at the surface in a) January and b) July.

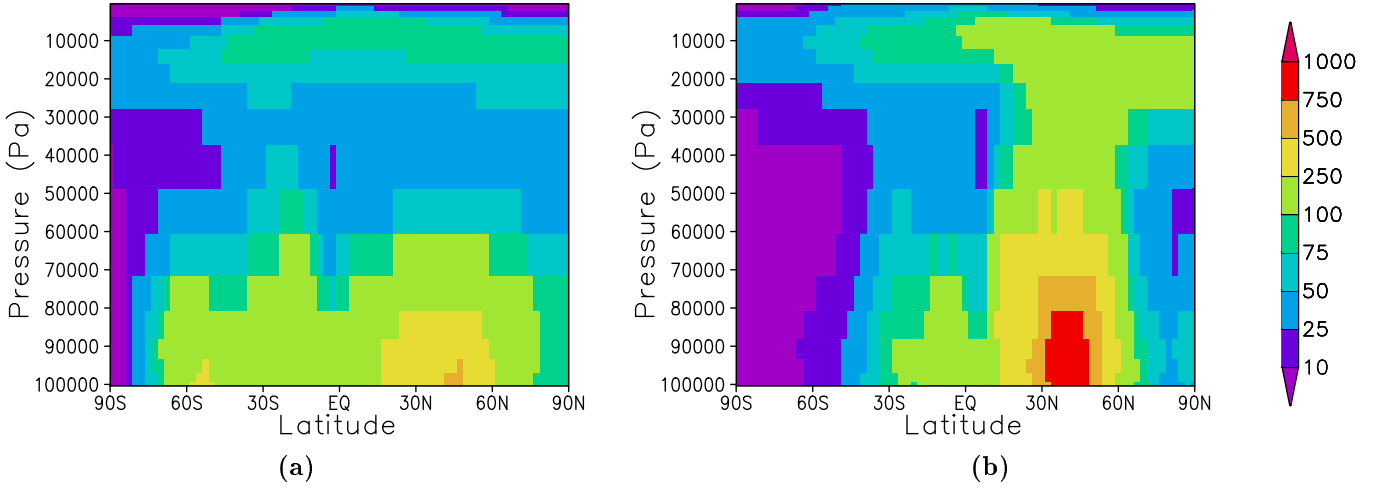


Fig. 5: Zonally-averaged mixing ratio of sulfate (pptv) in a) January and b) July.

ing sites. The present version of LMD-ZT represents typical conditions as opposed to specific meteorological situations. In order to assess the performance of this climatologically-driven model, we use data obtained at surface sites for a period of at least one year. These data include SO_2 and sulfate measurements from the European Monitoring and Evaluation Programme (EMEP) for Western Europe (see Aas et al., 1999) and the Eulerian Model Evaluation Field Study (EMEFS) for North America (see McNaughton and Vet, 1996). We use data from years 1980–1990 and 1988–1990 for EMEP and EMEFS, respectively. Model results are also compared to surface data from some remote oceanic sites (mostly those of the Sea-Air Exchange program (SEAREX)).

We also compare the model results with data obtained during three aircraft field campaigns which took place in the Pacific Ocean: Pacific Exploratory Mission (PEM)-West A (September–October 1991), PEM-West B (February–March 1994), and PEM-TROPICS-A (August–October 1996). Although these measurements are only representative of a region during the time period of the flights, they enable us to examine the vertical and horizontal distributions of the modelled sulfur species and identify any potential systematic biases.

4 Surface Concentrations of Sulfur Species

The surface distributions of the mixing ratios of DMS, SO_2 , and sulfate are presented in Figs. 2–4, respectively. The mixing ratio of DMS at the surface exhibits the same seasonal variation as the emission strength. It is maximum at 50–70°S in January and over the North Pacific and the North Atlantic Oceans in July (Fig. 2). The mixing ratio of SO_2 is largest over the continents and close to the regions of emission (Fig. 3). It shows few differences between January and July, except over the mid-latitudes of the Southern Hemisphere where oxidation of DMS is the main source for SO_2 . The spatial distributions of SO_2 and sulfate mixing ratios show some similarities but differ

in that sulfate aerosols spread further away from the regions of emissions of industrial SO_2 (Fig. 4), as expected from the longer lifetime of sulfate aerosols compared to SO_2 (see section 7). We could also note from Fig. 5 that sulfate aerosols spread vertically into the free troposphere during summertime.

Table 4: Comparison of modelled versus observed annually-averaged concentrations at the surface

Location	Observed ^a	Modelled ^a
<i>DMS</i>		
Cape Grim	65	50
Amsterdam Island	181	118
<i>SO₂</i>		
EMEP sites (<50°N)	3945	4306
EMEP sites (>50°N)	3037	3528
EMEFS sites	3038	5460
Amsterdam Island	18	20
<i>Sulfates</i>		
EMEP sites (<50°N)	1588	1284
EMEP sites (>50°N)	1166	895
EMEFS sites	1252	1449
Oceans (NH) ^b	225	177
Oceans (SH) ^c	80	101
Antarctic ^d	25	33
<i>MSA</i>		
Arctic ^e	6	1
Oceans (NH) ^f	8	5
Oceans (SH) ^c	5	7
Antarctic ^g	9	4

^aValues are in pptv.

^bBarbados, Belau, Bermuda, Fanning, Guam, Mace Head, Midway, and Oahu.

^cAmerican Samoa, Cape Grim, New Caledonia, and Norfolk.

^dMawson, Palmer, and the South Pole.

^eAlert and Heimaey.

^fBarbados, Bermuda, Fanning, Mace Head, Midway, and Oahu.

^gMawson and Palmer.

Table 4 presents a comparison of modelled and observed mixing ratios of DMS, MSA, SO_2 , and sulfate; the data are annual-mean mixing ratios averaged over the remote and polluted monitoring stations given in the table caption. Model results are within a factor of 2 of measurements, except for MSA which is underestimated by as much as a factor of 6 in the Arctic and Antarctic sites.

This matter should be investigated in the future, by considering direct MSA production from DMS and not from DMSO. In the following subsections, we show the modelled versus observed mixing ratios at some representative sites in order to illustrate and discuss the performance of the model in terms of seasonality.

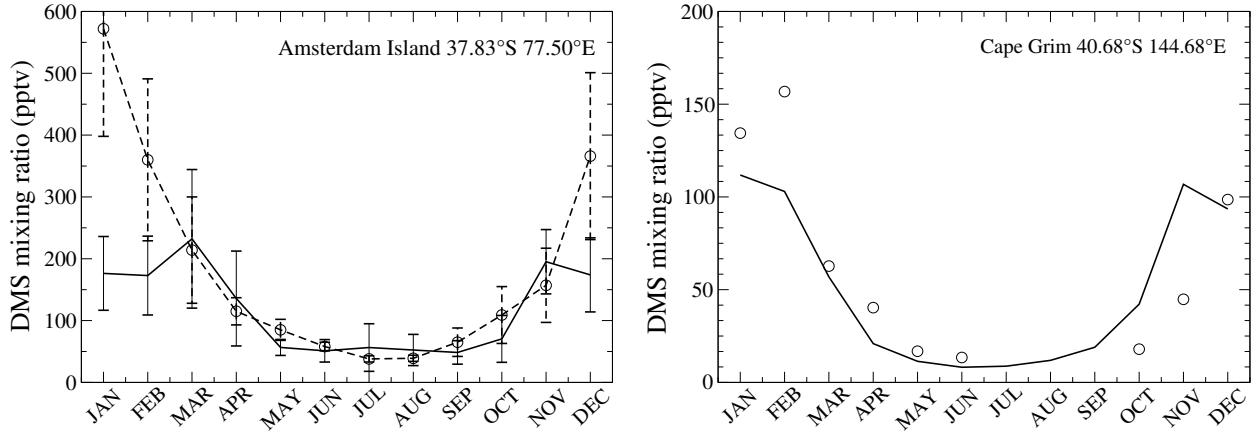


Fig. 6: Seasonal variations in surface DMS (pptv) at Amsterdam Island and Cape Grim. The open circles and the solid line indicate the monthly-mean observed and modelled mixing ratios, respectively.

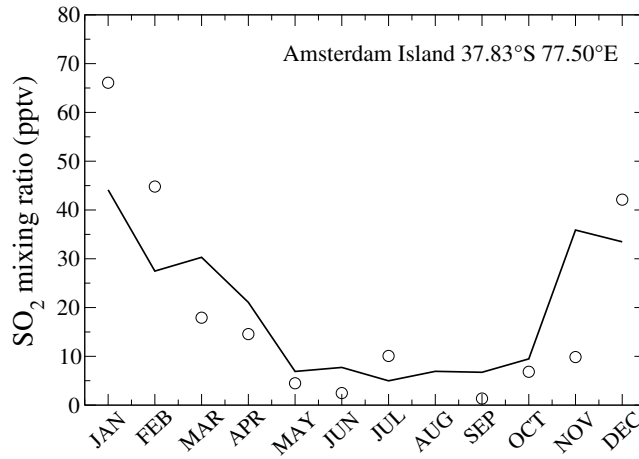


Fig. 7: Seasonal variations in surface SO_2 (pptv) at Amsterdam Island.

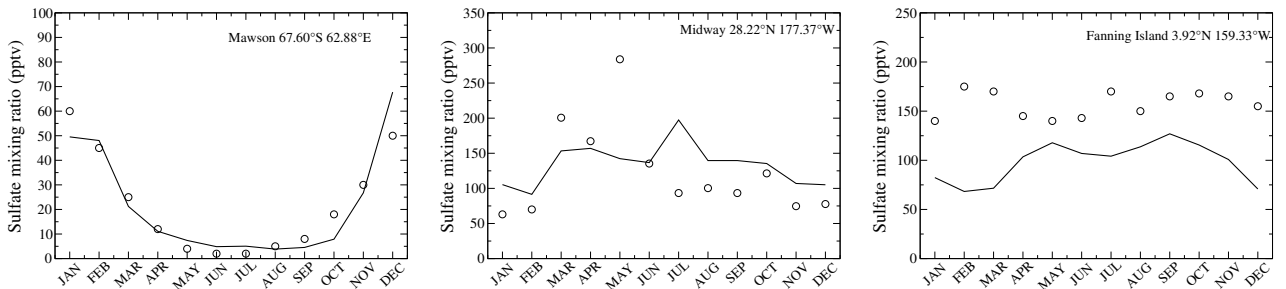


Fig. 8: Seasonal variations in surface sulfate (pptv) at Mawson, Midway, Fanning Island, and Cape Grim.

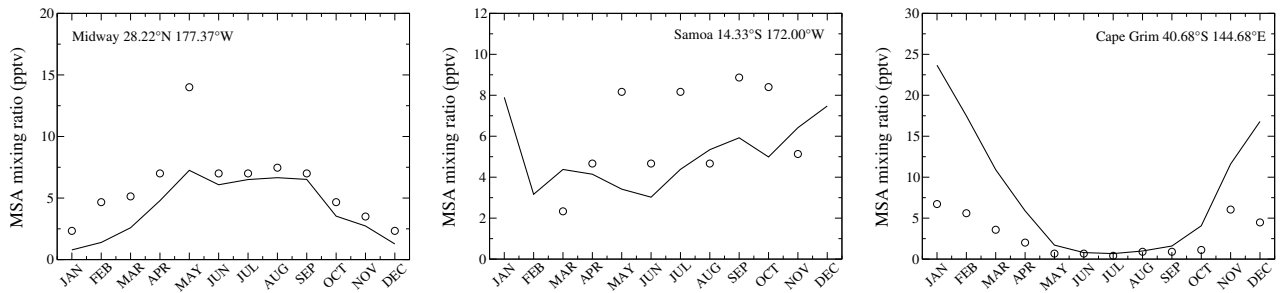


Fig. 9: Seasonal variations in surface MSA (pptv) at Midway, Samoa, and Cape Grim.

4.1 Remote oceanic sites

Fig. 6 shows DMS mixing ratios at Amsterdam Island (Sciare et al., 2000) and Cape Grim. Observed mixing ratios at the two sites are characterized by a maximum in summer and a minimum in winter. This cycle is reproduced by the model for DMS, whose variation is intimately related to the variation of DMS emission flux at the two sites. For this compound, the agreement with the observations is good from March to November at Amsterdam Island and March to October at Cape Grim. The model underestimates the summer (January-February) peak in concentration at both sites. A more complete investigation of DMS emission flux and concentration in the southern hemisphere using this model is provided in Cosme et al. (2002). The calculated mixing ratios exhibit a peak which is not observed in the measurements at the two sites. This peak reproduces a similar peak in the DMS emission flux, which may be an artifact due to the very low density of data in the Southern Indian Ocean used in the emission mapping procedure of Kettle et al. (1999).

As showed in Fig. 7, the seasonal cycle of SO_2 at Amsterdam Island is well reproduced if we compare the model results to the data of Putaud et al. (1992). At this site, SO_2 is mainly produced by DMS oxidation. The modelled SO_2 mixing ratio, similarly to DMS, is also overestimated in November but underestimated in January.

Fig. 8 presents comparisons for sulfates at some remote oceanic sites. Two of them (Mawson and Midway) are characterized by large seasonal variations, while Fanning Island does not show any remarkable seasonality. At Cape Grim (not shown), nss-sulfates are overestimated by a factor of more than 5 when compared to measurements by Ayers et al. (1991), while DMS mixing ratios compare well with the observations. Since observations correspond to ‘baseline’ or clean conditions only, while our results also include anthropogenic sulfates coming from the continent,

the discrepancy between model and observation is therefore not meaningful. Note, however, that measurements reported by Andreae et al. (1999), also for baseline conditions, are significantly higher than those of Ayers et al. (1991), reducing the discrepancy. The absence of seasonal variation at Fanning Island is reproduced by the model, though the modelled values are underestimated by a factor of 2, as well as the seasonality of the observed mixing ratios at Mawson. The modelled ratio of the summertime to wintertime values is 12 at Mawson, versus 17 for the observations. The agreement is poorer for the Midway station, where the model does not seem to simulate adequately the transport of Asian pollutants during spring.

As shown on Fig. 9, the model captures well the MSA concentrations at Samoa and Midway, within a factor of 2. At Cape Grim, MSA mixing ratios are largely overestimated in summer, while modelled DMS mixing ratios agree rather well with the observations. The agreement is better if we use the data of Andreae et al. (1999), with observed MSA mixing ratios peaking at about 14 pptv in February.

4.2 Continental/Polluted areas

Most of the monitoring stations are located in Europe (EMEP network) and Northern America (EMEFS network) and they report measurements of SO_2 and sulfate concentrations in air, sulfate concentration in rainwater, and precipitation (see Fig. 10). The results for the EMEP and EMEFS stations are summarized as scatter plots in Figs. 11 to 14. For each plot, each point represents the modelled and observed monthly-mean values at one site in January, April, July, and October (a model grid-box can occasionally be compared to several sites if their geographical distance is less than the horizontal resolution of the model).

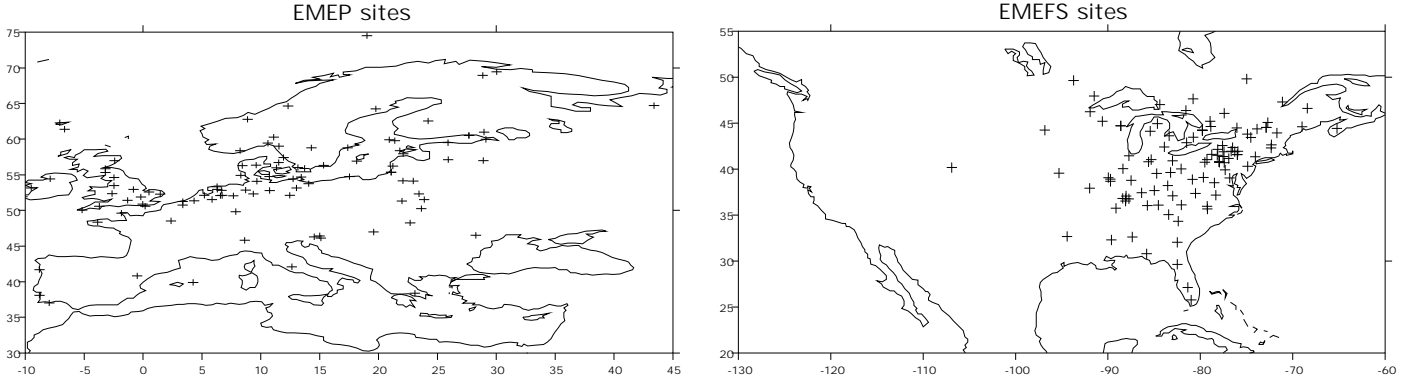


Fig. 10: Geographic distribution of the EMEP and EMEFS sites used in this study.

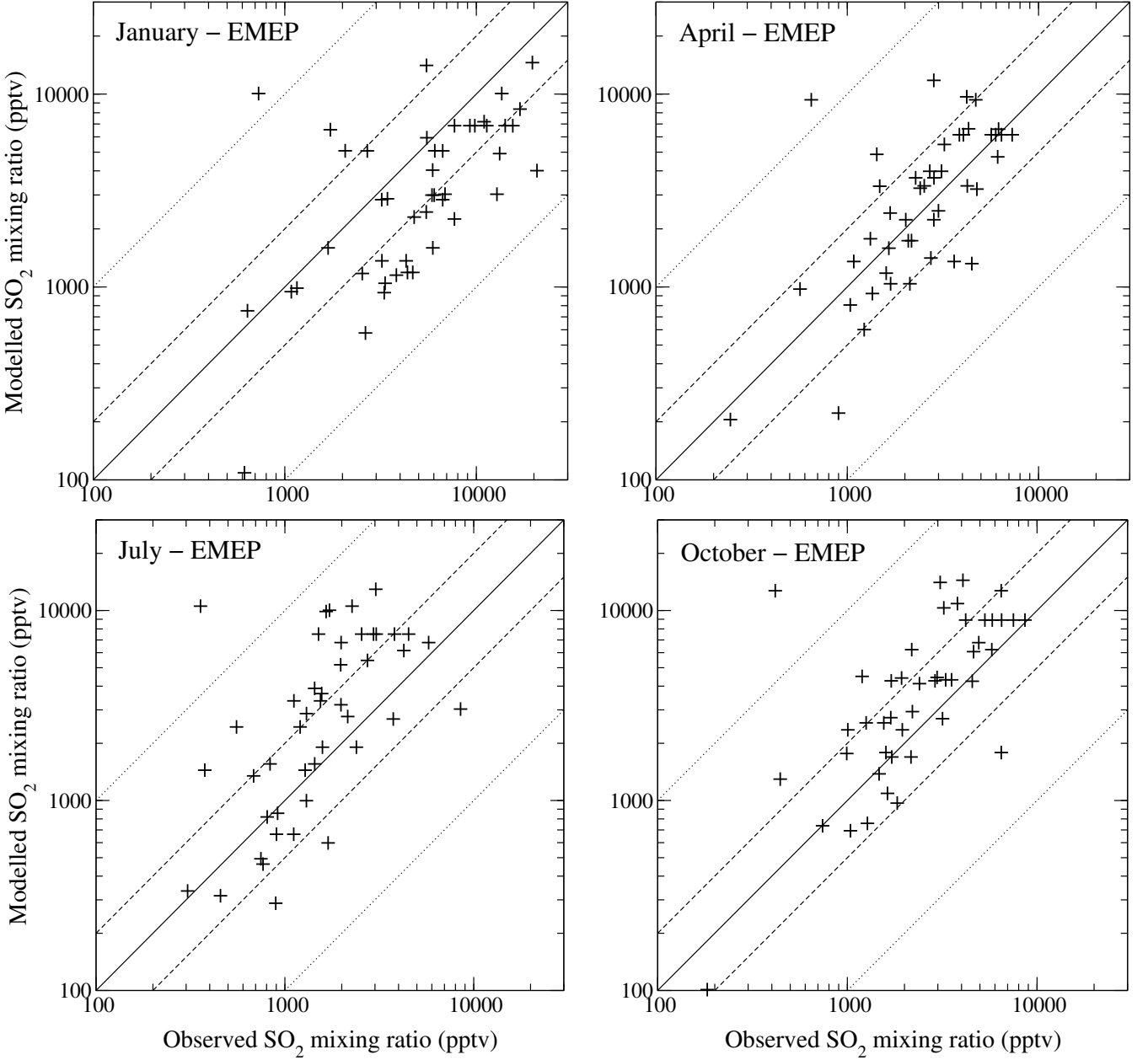


Fig. 11: Scatter plot of measured vs modelled SO_2 mixing ratios (pptv) at EMEP surface sites in January, April, July, and October. The 1:1 line (solid), the 1:2 and 2:1 lines (dashed), and the 1:10 and 10:1 lines (dotted) are shown for reference.

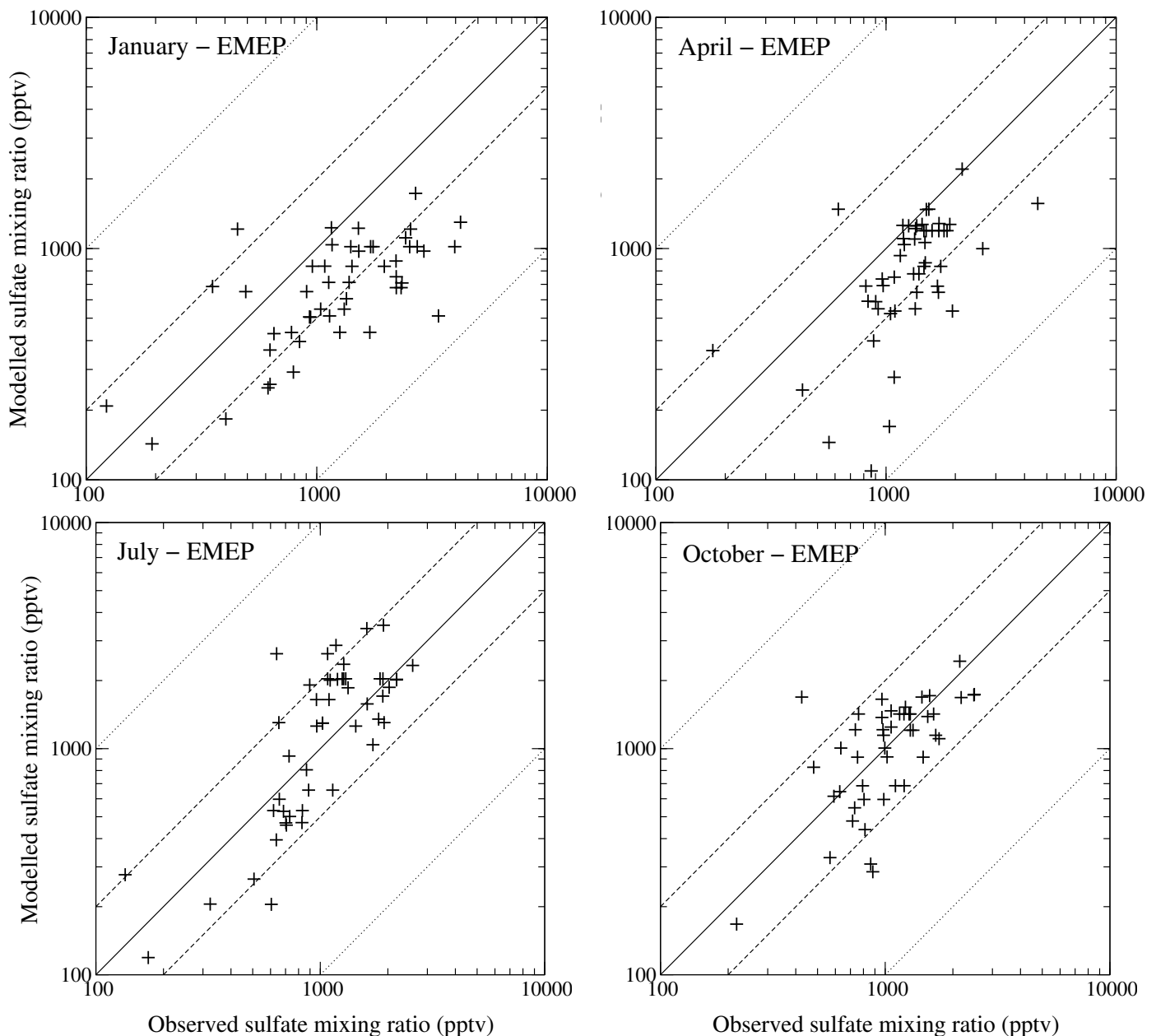


Fig. 12: Same as Fig. 11 but for sulfate.

Modelled and observed SO_2 mixing ratios are evenly distributed around the 1:1 line in April over Europe and in January over Eastern North America. In both regions SO_2 mixing ratios are overestimated in July and October. They are also underestimated in January over Europe, which is opposite to the recent model results of Koch et al. (1999) and Barth et al. (2000). The overestimates in July and October are probably due to a too weak SO_2 conversion into sulfates since precipitation and cloud cover are underestimated in the model at these periods of the year.

In order to discuss the behavior of the model at different latitude and longitude bands, we also display on Fig. 15 the observed and modelled seasonal cycles at some representative sites in Europe and North America. The underestimate of SO_2 in winter is illustrated on the first row of Fig. 15 with the sites of Cree Lake, Aspveten, and

Krvatn, which are all north to 50°N . At these high latitudes areas, the winter discrepancy might be related to either an insufficient transport of sulfur to the high latitudes, either a too high deposition rate for SO_2 , or, a too strong in-cloud oxidation of SO_2 by O_3 . In summer modelled SO_2 mixing ratios compare rather well with observations (less than a factor 2). Going further south, modelled SO_2 is overpredicted from March to December over Europe and North America with slight peaks occurring in August, September, and November (middle row of Fig. 15). The agreement is satisfactory in the latitude band $25\text{--}35^\circ\text{N}$ (last row of Fig. 15), where the seasonal variations are respected within a factor of 2 to 3.

The large degree of variability among observed values should be noted. Although distant of less than 2° in latitude and longitude, the observed January maxima at Whiteface and Warwick are less than 3000 pptv and

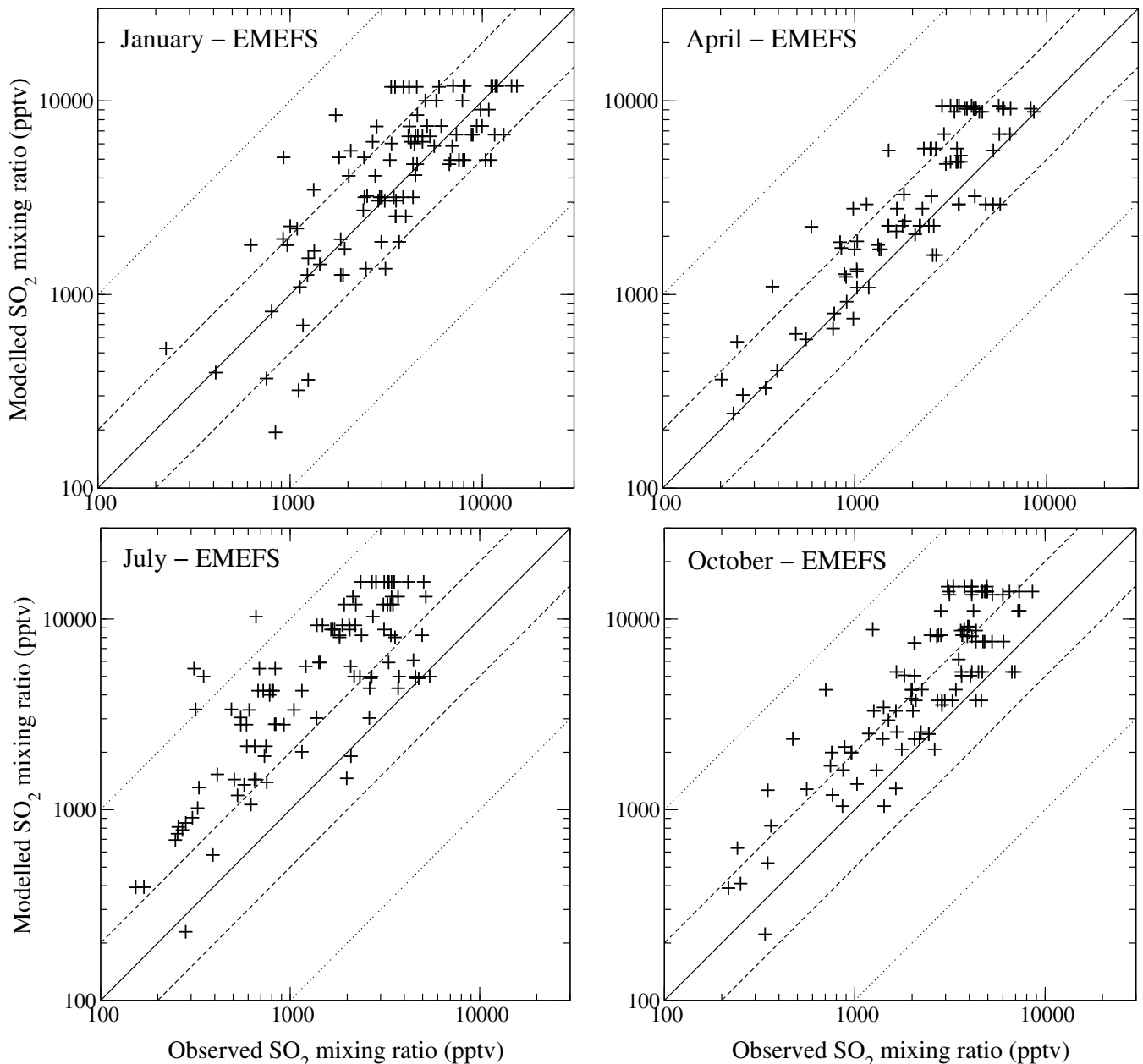


Fig. 13: Same as Fig. 11 but for EMEFS surface sites.

more than 5500 pptv, respectively. Similarly a maximum of 5300 pptv has been observed at Bells (around 35°N, 89°W), while the maximum only reaches 1500 pptv at Caryville (around 30°N, 86°W). The model reproduces satisfactorily these gradients in concentrations.

For the continental EMEP and EMEFS stations, most modelled and observed sulfate mixing ratios agree within a factor of 2, except for January and April in Europe (Fig. 12 and Fig. 14). There is a tendency to underestimate the concentrations over Europe in January and April and a slight tendency to overestimate concentrations over America in January and October. As far as EMEFS October data are concerned, this does not necessarily contradict the explanation given above that SO_2 to sulfate conversion rates are too slow. Both SO_2 and sulfate can be overestimated because a too low cloud cover and precipitation rate would result at the same time in too slow a conversion

rate of SO_2 and too low a wet scavenging of sulfate. One striking feature of the figures is the large underestimate of sulfates in January and to a lesser extent in April over Europe. This discrepancy is probably due to a too large precipitation rate over Europe in winter maybe associated with a too large transport outside of the boundary layer. It is unlikely to be solely due to an insufficient conversion rate of SO_2 into sulfates, as SO_2 is underestimated in January.

Fig. 16 presents the seasonal behavior of sulfate at the same sites as SO_2 . In mid-latitudes over the United States, the sulfate is observed to be highest in July-August. The model tends to give the same behaviour. At Montelibretti, wintertime sulfate mixing ratios are underestimated, due to an insufficient wintertime SO_2 oxidation and/or an excessive sink. North to 50°N, the agreement is within a factor of 2 to 3 although the high mixing ratios of sulfate

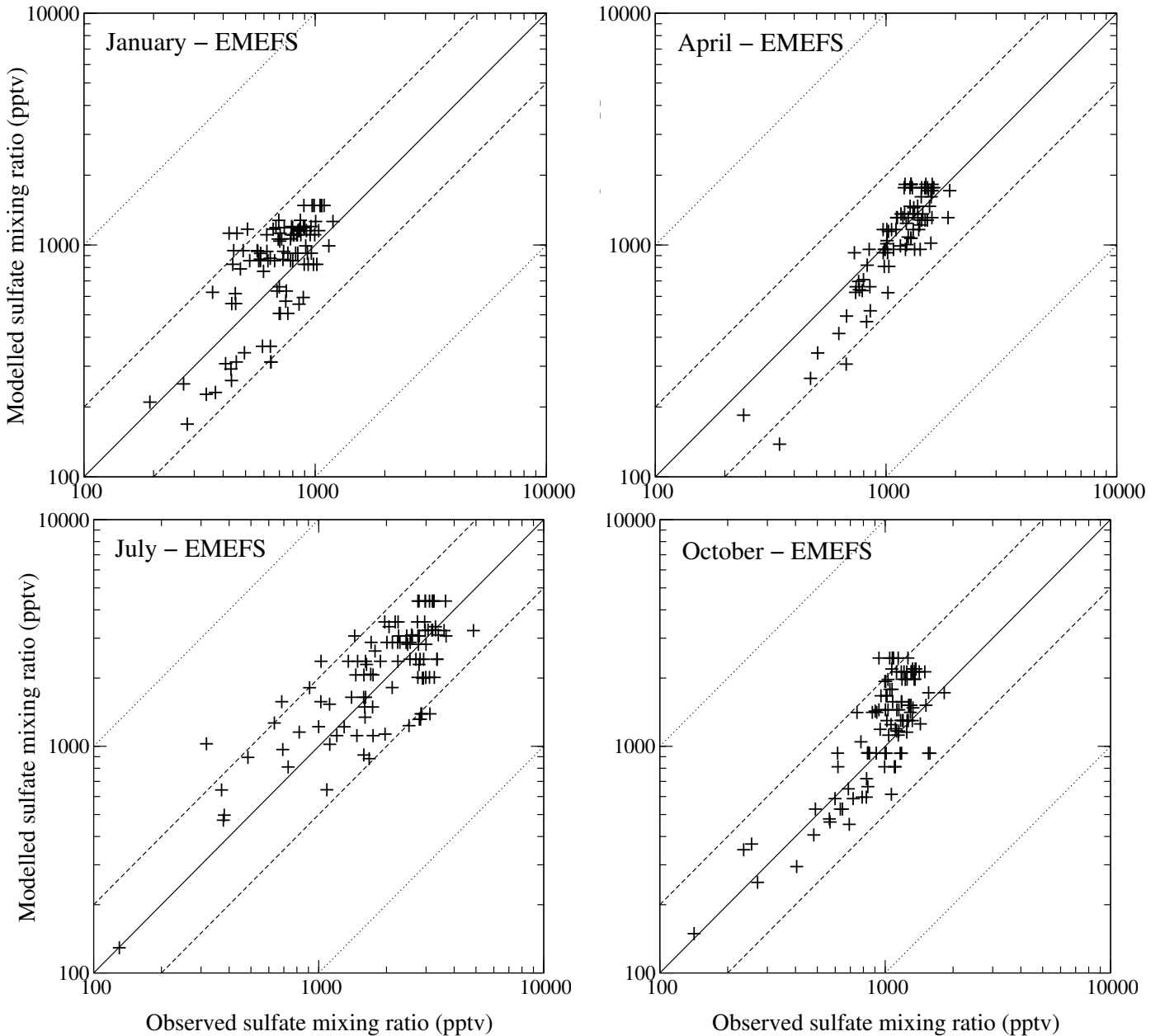


Fig. 14: Same as Fig. 12 but for EMEFS surface sites.

at springtime are not reproduced by the model at neither three locations.

5 Vertical Profiles of Sulfur Species

This section assesses the model performance in the middle and high troposphere. The data used for the comparison between modelled and observed values have been collected during the PEM campaigns and have been grouped into regions using the same classification as Barth et al. (2000). The data from the different flights have been merged and averaged over nine given regions at each model vertical layer. The model results have been averaged over the selected regions and over the measurement pe-

riod: February-March for the PEM-West B intensive campaign, September-October for the PEM-West A and PEM-Tropics-A campaigns. Note that the PEM-Tropics-A took place further east in the Pacific Ocean. It should also be noted that the model results represent a climatological situation which does not necessarily correspond to the local meteorological conditions and does not reproduce the variability in the mixing ratios as observed during the time periods of the PEM campaigns.

5.1 DMS

Observed DMS mixing ratios (Fig. 17) vary from around 20–40 pptv at the surface and decrease rapidly with altitude in the PEM-West A and B campaigns. This is well reproduced by the model. Nevertheless, in some cases,

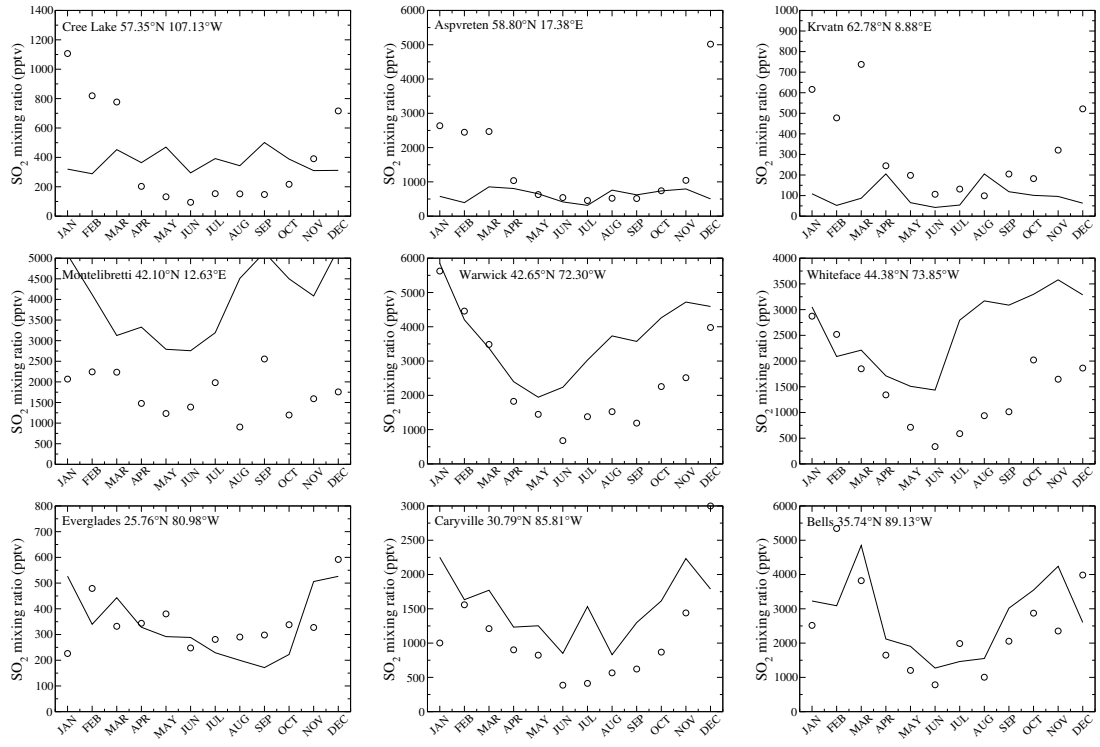


Fig. 15: Seasonal variations in SO_2 mixing ratio (pptv) at selected sites of the EMEP and EMEFS networks. The open circles and the solid line indicate the monthly-mean observed and modelled mixing ratios, respectively. Note that different plots have different scales on the y-axis.

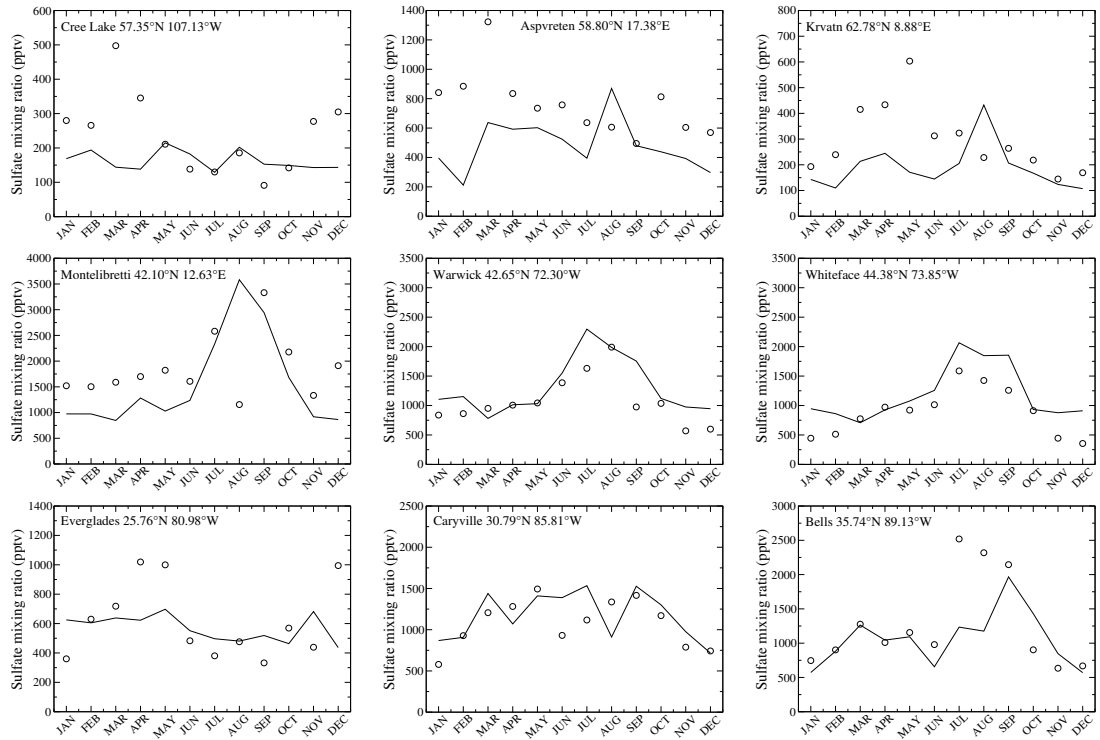


Fig. 16: Seasonal variations in sulfate mixing ratio (pptv) at selected sites of the EMEP and EMEFS networks. The open circles and the solid line indicate the monthly-mean observed and modelled mixing ratios, respectively.

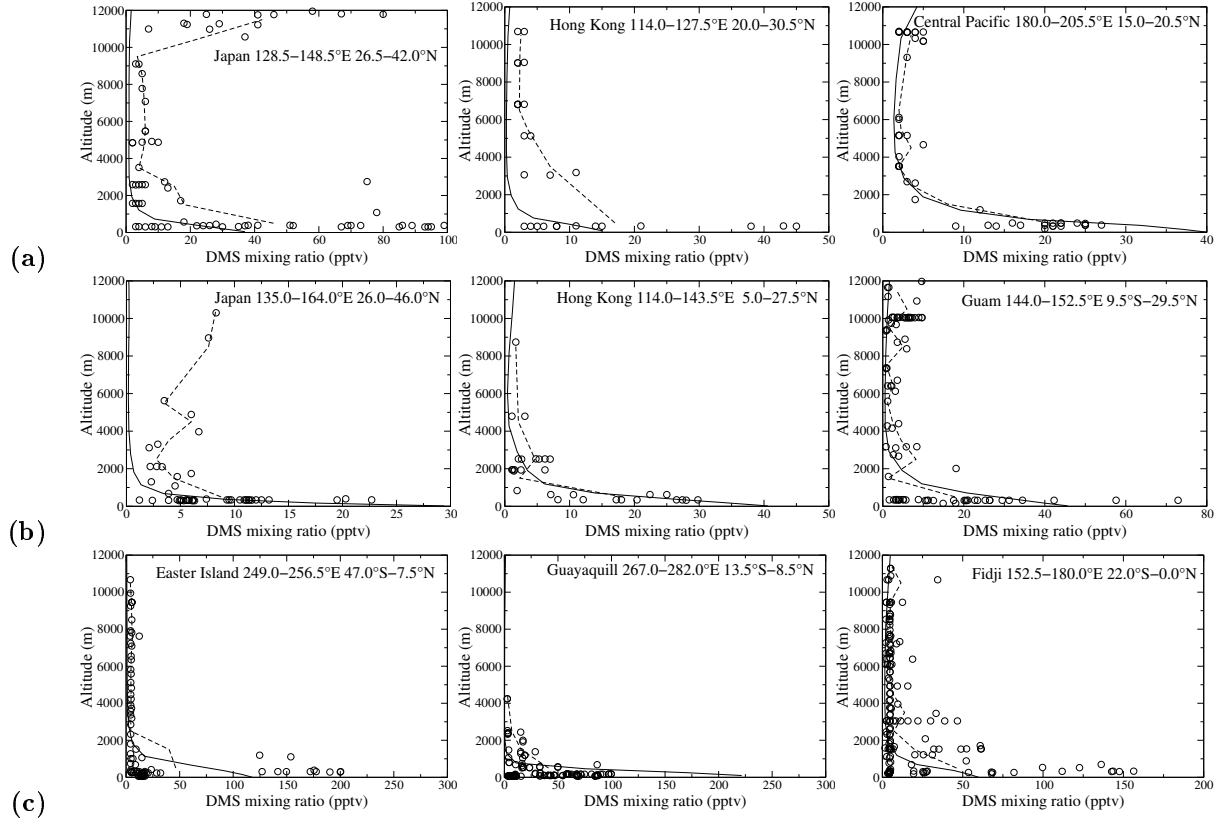


Fig. 17: DMS mixing ratios versus height during a) the PEM-West A, b) PEM-West B, and c) PEM-Tropics A field campaigns. Model results averaged over the region and period of the measurements are indicated by a solid line. The observed mixing ratios averaged in altitude bands of 1 km are also shown with a dashed line.

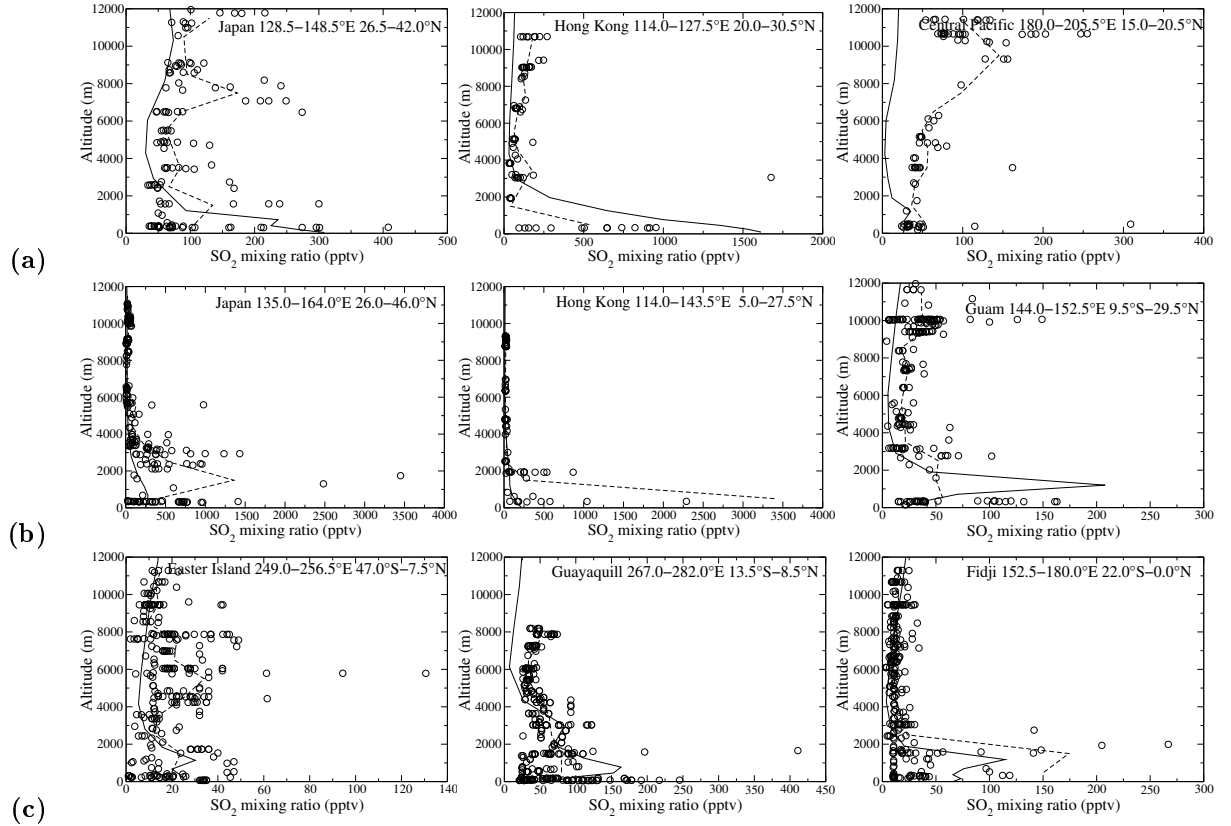


Fig. 18: Same as Fig. 17 but for SO_2 .

modelled mixing ratios are too low in the upper troposphere, where DMS may be pumped up by convective activity with mixing ratios reaching more than 10 pptv (see the Japan area during autumn and early spring, and the Guam area). In the Eastern Pacific (PEM-Tropics A), DMS mixing ratios are higher than in West-A and B (more than 50 pptv at the surface) and decrease rapidly with altitude. The model is in fair agreement with these profiles, except for the surface, where modelled DMS concentrations are overestimated in two cases.

In the Eastern Pacific (PEM-Tropics A), DMS mixing ratios are higher than in West-A and B (more than 50 pptv at the surface) and decrease rapidly with altitude. The model is in fair agreement with these profiles, except for the surface, where modelled DMS concentrations are overestimated in two cases.

5.2 SO₂

SO₂ mixing ratios observed during PEM-West A increase, are constant, or decrease with altitude (Fig. 18). In Japan and Hong-Kong, the model is in good agreement with the observations, but in two cases it tends to overestimate the surface concentrations. Over Central Pacific on the other way, it is below the observed mixing ratios of 100–200 pptv in the high troposphere, which is probably due to long-range transport and convective activity, or return

injection of volcanic SO₂ from the stratosphere (Thornton et al., 1996). Peaks of SO₂ are also observed in the boundary layer and free troposphere of the PEM-West B area. The model does not represent properly the transport of pollutants from Asia during spring 1994 at the surface, with too low modelled mixing ratios, except for the Guam area. In the Eastern Pacific (PEM-Tropics A), surface observed mixing ratios are lower than in the western regions, and the observed peaks of SO₂ in the boundary layer are reproduced by the model.

In summary, except for the Central Pacific area, the model reproduces the high mixing ratios in the middle and high troposphere. At the surface, the agreement is within a factor 3.

5.3 Sulfates

The agreement between observations and model results of sulfates is variable (Fig. 19). In the boundary layer, the model sometimes underestimates (Hong-Kong area in spring, Guayaquil area in autumn), and sometimes overestimates (Japan and Central Pacific in autumn, Guam in spring) the observed values. In the middle and high troposphere, modelled mixing ratios of sulfates are either too high (Japan in autumn or Fidji) or in agreement (Central Pacific, Japan and Hong-Kong in spring, Easter Island, or Guayaquil).

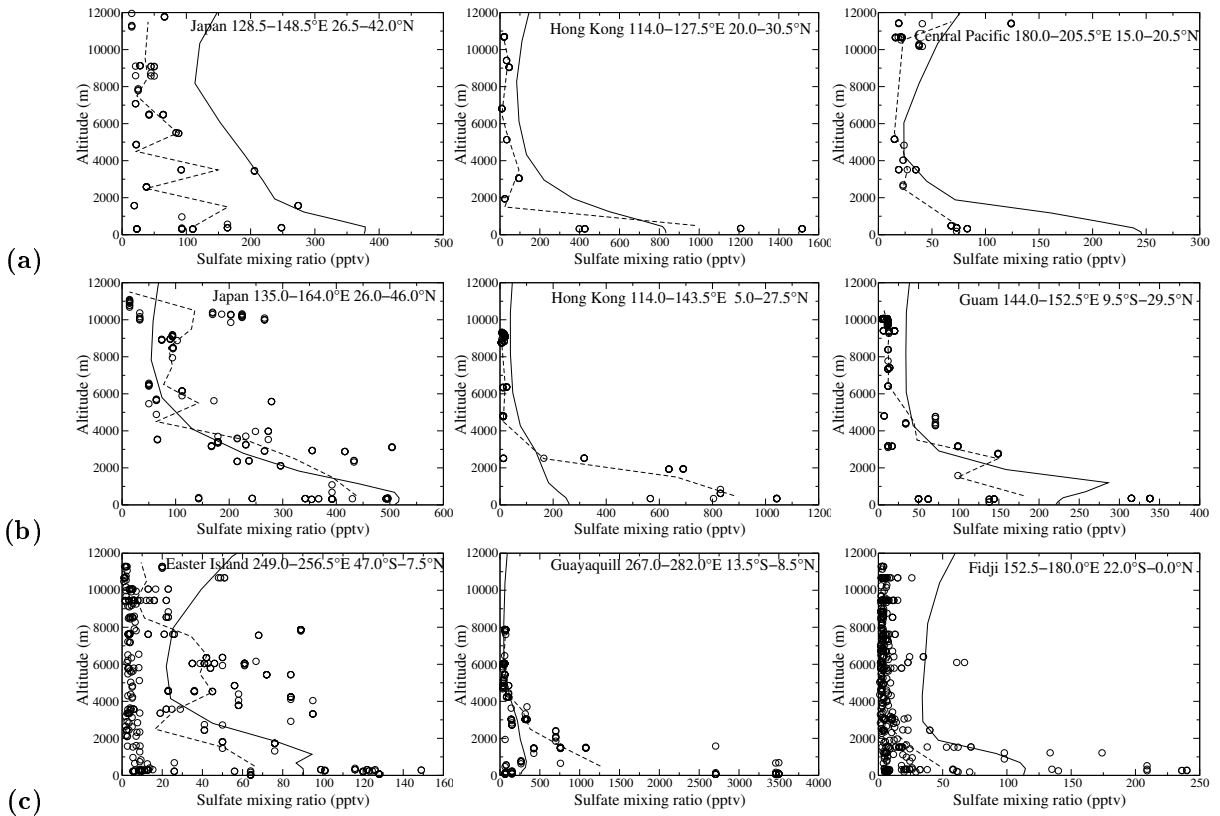


Fig. 19: Same as Fig. 17 but for sulfates.

6 H₂O₂ distribution

The surface (Fig. 21) and zonal (Fig. 22) distribution of the H₂O₂ mixing ratio is in broad agreement with that simulated by other global models (e.g., Barth et al., 2000). There are nevertheless differences between the distribution of H₂O₂ simulated in IMAGES with a full chemical scheme (excluding, however, in-cloud oxidation of SO₂) and that simulated here with a simplified chemical scheme (but including in-cloud oxidation of SO₂). Surface H₂O₂ mixing ratios are larger in IMAGES than in LMD-ZT at high latitudes (north to 45°N and south to 50°S) during January, but are rather similar in July. Over the Northern midlatitudes, the simulated mixing ratios in LMD-ZT are much smaller in wintertime than in summertime, which explains the lower oxidation rate of SO₂ by H₂O₂ in winter. Note also that the largest mixing ratio of H₂O₂ are not found at the surface but at a higher altitude, as observed in field campaigns.

The concentration of H₂O₂ has been measured in several field campaigns (MLOPEX II, PEM, and TRACE) but is not monitored as that of sulfur species. Over continental regions of the Northern Hemisphere, the compilations of Lee et al. (2000) and Grossmann (1999) show that available measurements of H₂O₂ are scarce. In particular, there does not seem to be any measurements of

H₂O₂ concentration over Europe in winter.

Table 5 shows a comparison between modelled and measured values of H₂O₂ at long-term (at least one year) monitoring sites as cited by Lee et al. (2000). Except for Cape Grim, where the observed amplitude of the seasonal cycle is more than twice the modelled one, the ratio winter/summer is well represented. The model underestimates the observed concentrations by Boatman et al. (1989) over Central U.S. but is in the range of the measurements made by Van Valin et al. (1987) during the CURTAIN (Central U.S. RADM Test and Assessment Intensives) campaign which took place in the same area in February 1987. Typical modelled values range from 0.02 to 1.2 ppbv from north (40.5°N) to south (29°N) along the 91.5°W meridian and are within the range of measurements: < 0.01 to 1 ppbv with an increase of 0.04–0.05 ppbv per degree of latitude from North to South.

Over the United States in winter, comparison with measurements by Barth et al. (1989) shows a fair agreement below 3 km, but an overestimate by a factor of about 3 above 3 km. On the other hand, the modelled profile of H₂O₂ is underestimated by a factor of 2 to 4 in October–November over the eastern United States compared to the measurements given by Heikes et al. (1987).

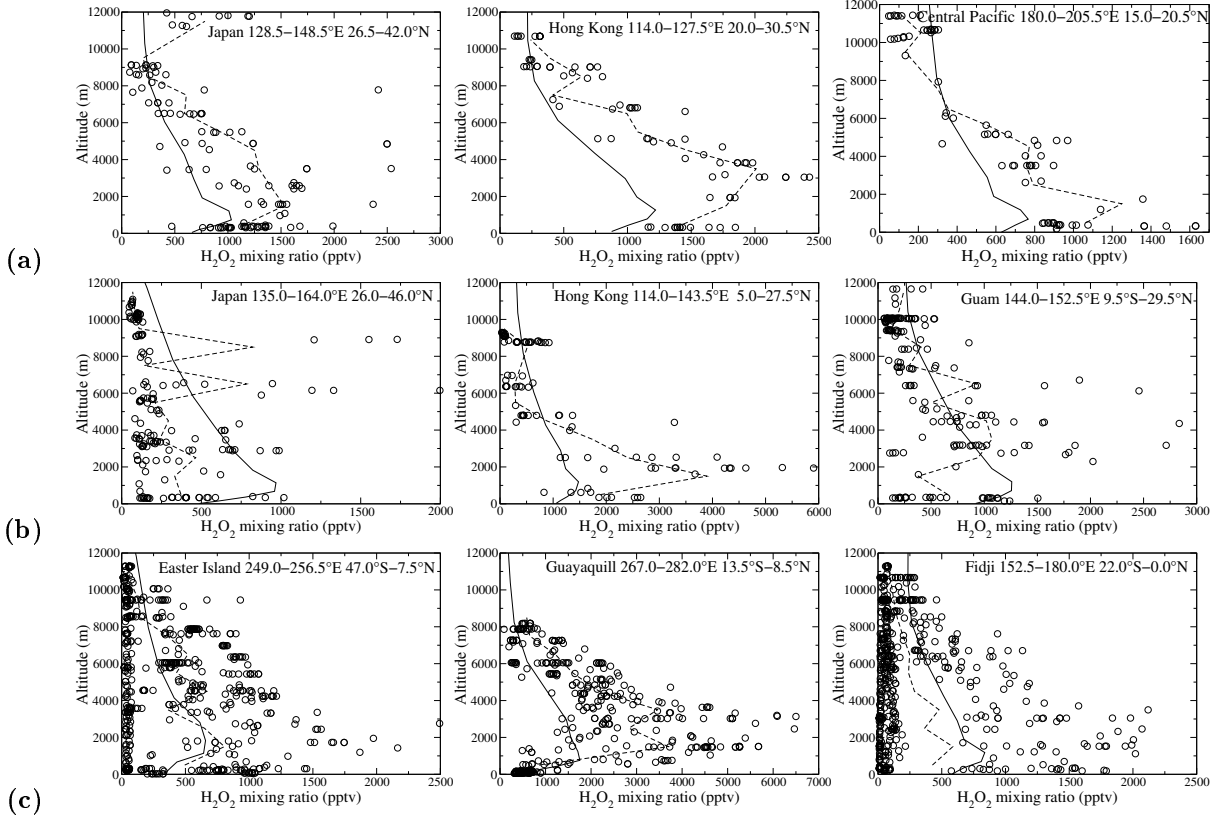
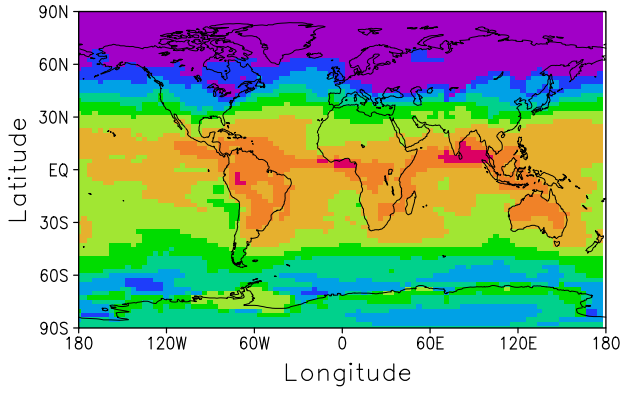
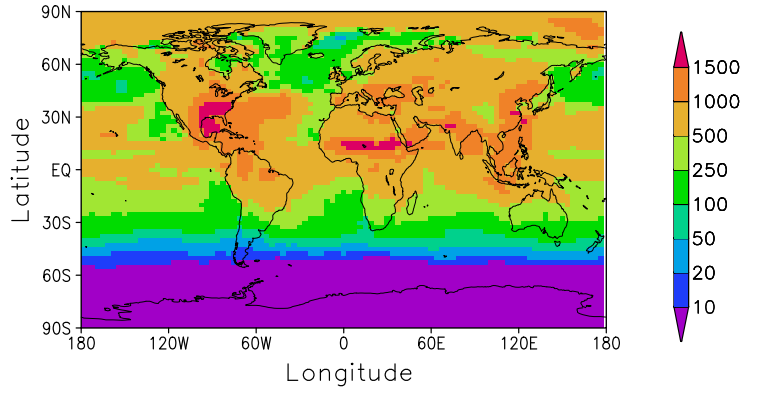


Fig. 20: Same as Fig. 17 but for H₂O₂.

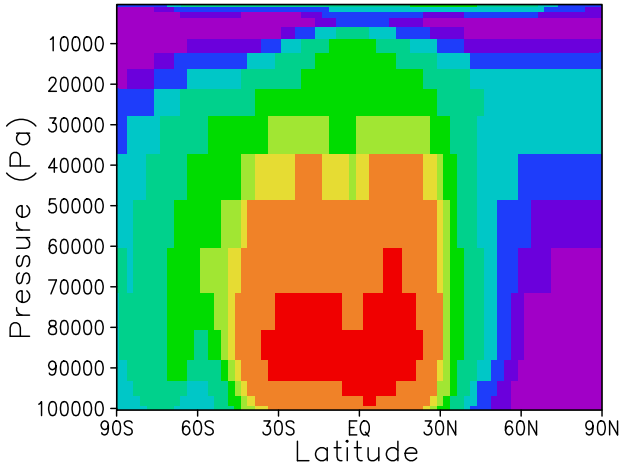


(a)

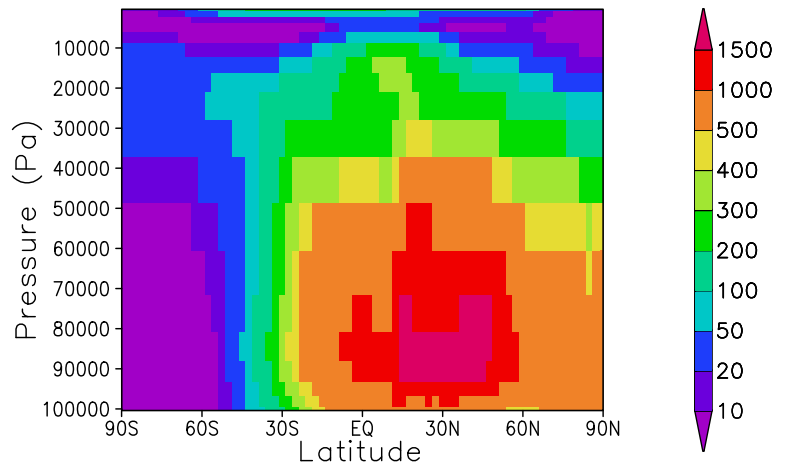


(b)

Fig. 21: Distribution of predicted H_2O_2 mixing ratio (pptv) at the surface in a) January and b) July.



(a)



(b)

Fig. 22: Zonally-averaged mixing ratio of predicted H_2O_2 (pptv) in a) January and b) July.

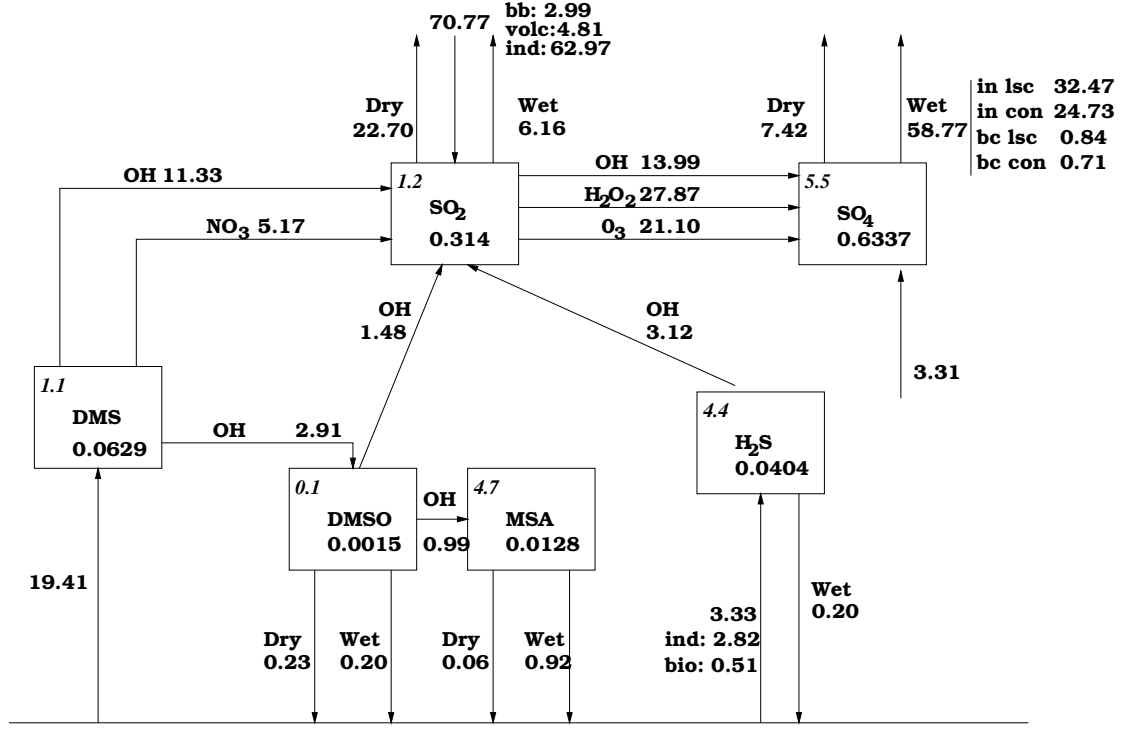


Fig. 23: Globally- and annually-averaged sulfur budget. Burdens are given in Tg S, fluxes in Tg S yr⁻¹, and lifetimes (in italics) in days. Dry and Wet stands for dry and wet depositions, respectively. Wet deposition is due to in-cloud (in) and below-cloud (bc) scavenging from large-scale (lsc) and convective (con) clouds.

The measured H₂O₂ mixing ratios during the PEM campaigns are in broad agreement with the simulated ones (see Fig. 20). The model reproduces the increase of mixing ratios in the boundary layer as observed during most of the campaigns.

Since H₂O₂ long-term measurements are scarce, it is difficult to draw any definite conclusion about the representation of H₂O₂ in our model. Measurements of H₂O₂ over Europe are also greatly needed to resolve the issue of wintertime underestimation of sulfate concentrations.

Table 5: Comparison of modelled versus observed H₂O₂ mixing ratios (ppbv) at long-term stations.

Location	Observed Winter/ Summer	Modelled Winter/ Summer
Cape Grim	1.4/0.16 ^a	0.5/0.13
Los Angeles	0.2/1.0 ^b	0.2/0.7
Central U.S. (1.4–1.7 km)	0.3/4.1 ^c	0.14/1.6

^aAyers et al. (1996)

^bSakugawa and Kaplan (1989)

^cBoatman et al. (1989)

7 Budgets

Fig. 23 shows the budget of sulfur species on a global and annual average. The budget is in balance for all six

species. Except for in-cloud sulfate production and sulfate wet scavenging, all the terms of our sulfur budget are in the range of those given by Koch et al. (1999), Barth et al. (2000), and Chin et al. (2000a) (as compiled in Chin et al. (2000a)). Our in-cloud sulfate production and sulfate wet deposition are somewhat larger than those of these authors. In-cloud sulfate production is 49.0 Tg S yr⁻¹, in comparison to a range of 24.5 to 44.4 Tg S yr⁻¹ for the three studies cited above. For wet scavenging of sulfate, our model predicts a global- and annual-mean rate of 58.8 Tg S yr⁻¹, in comparison to a range of 34.7 to 51.2 Tg S yr⁻¹ for the same three studies.

DMS is oxidized primarily by OH to form SO₂ and DMSO, a smaller fraction being oxidized by NO₃.

SO₂ is depleted by dry deposition (24.7%), wet deposition (6.7%), oxidation in the gas phase (15.2%), and oxidation in the aqueous phase (53.3%). As shown on Fig. 24 which represents the distribution of the vertically-integrated sinks of SO₂ on a common colour scale, dry deposition is important over land, where SO₂ concentrations are large, but also over ocean, where the deposition velocity is larger. Oxidation by OH is more important in summer than in winter, in agreement with the seasonal variations in OH concentrations. Oxidation of SO₂ by O₃ is particularly important in wintertime at midlatitudes, but is supplanted by oxidation by H₂O₂ in summertime.

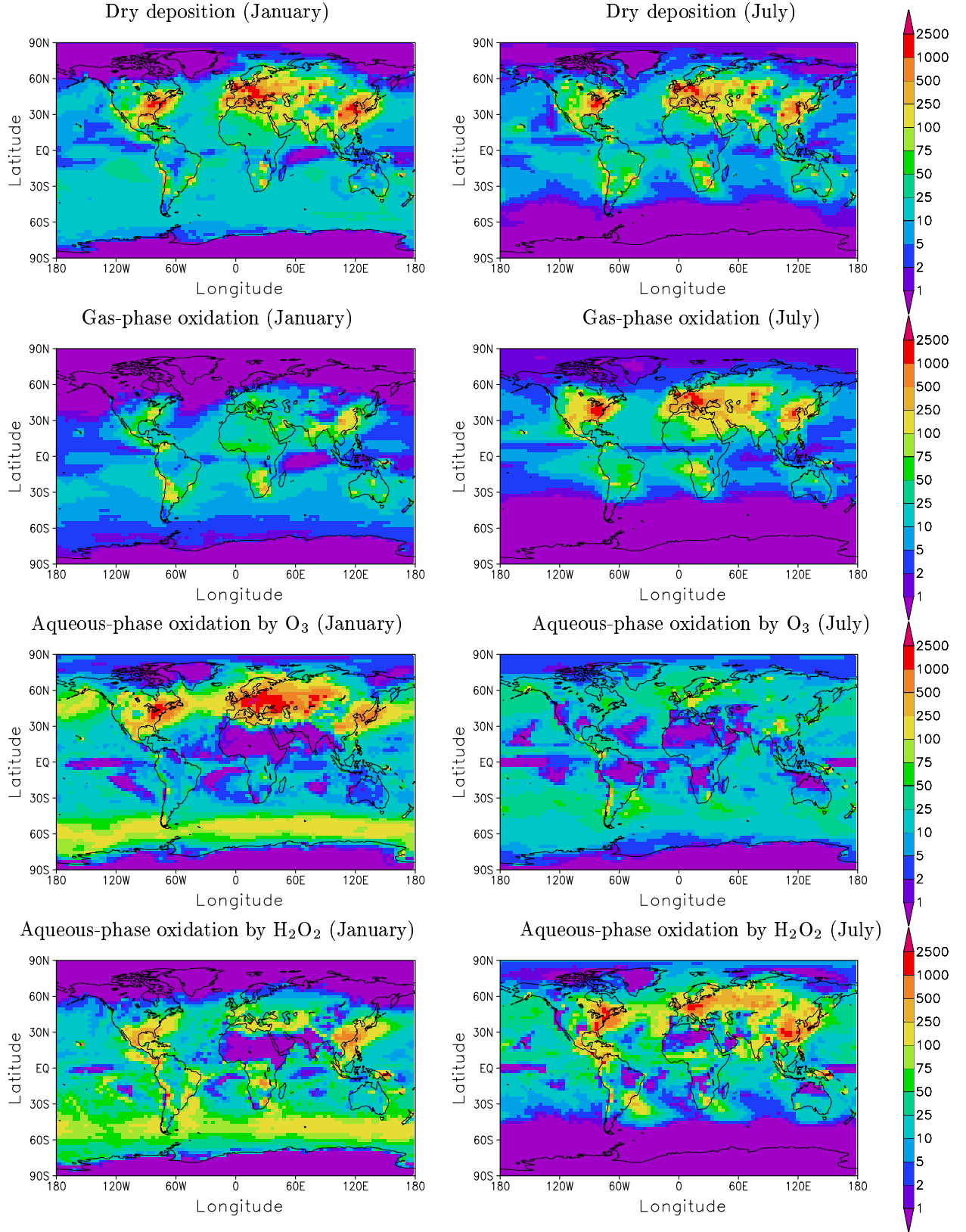


Fig. 24: Vertically-integrated sinks of SO_2 ($\text{mg S m}^{-2} \text{ yr}^{-1}$) in January (left) and July (right).

Sulfate sources include emissions (5.0%) and production by gas- and aqueous-phase oxidation of SO_2 (21.1% and 73.9%, respectively). Its main sink is through wet scavenging (88.8%), with a small contribution from dry

deposition (11.2%). In our model, in-cloud oxidation of SO_2 by O_3 plays a much larger role than in the studies of Feichter et al. (1996) and Barth et al. (2000). It amounts to 8.6% and 15.7% of sulfate production in these two

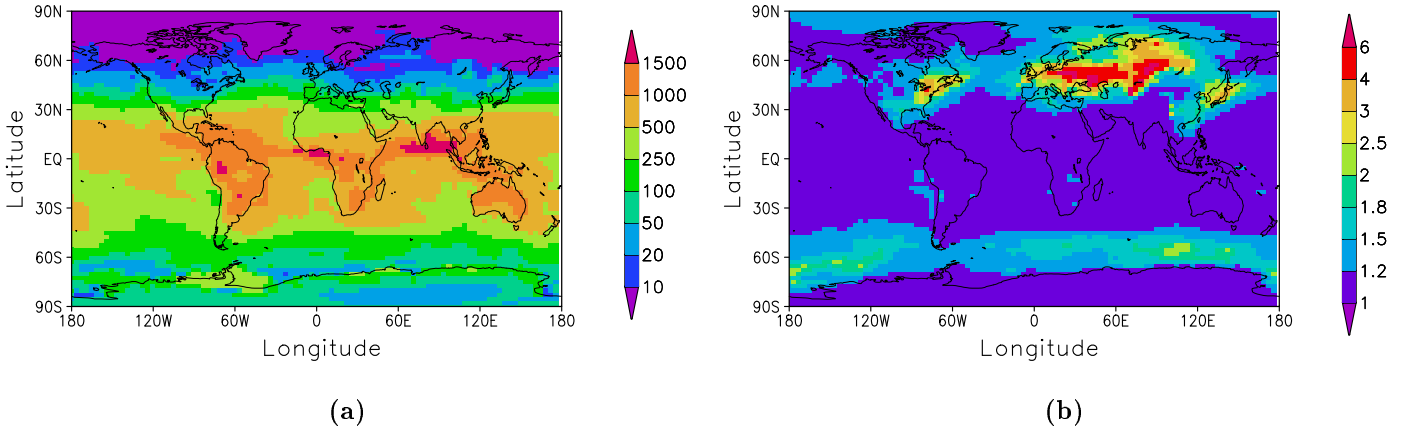


Fig. 25: a) Distribution of predicted H_2O_2 mixing ratio (pptv) at the surface in January in the simulation where H_2O_2 is not depleted upon oxidation of SO_2 (NODEPL). b) Ratio of January H_2O_2 mixing ratios between simulations where H_2O_2 is and is not depleted.

Table 6: Budget of H_2O_2 over the globe and over Europe.

		Global annual		Europe January ^a		Europe July ^a	
Burden ($\text{mg H}_2\text{O}_2 \text{ m}^{-2}$)		5.36		1.34		8.23	
Lifetime (days)		1.13		2.51		1.10	
Source ($\text{mg H}_2\text{O}_2 \text{ m}^{-2} \text{ yr}^{-1}$)	$\text{HO}_2 + \text{HO}_2$	1735.3	(100.0%)	191.0	(97.9%)	2737.4	(100.0%)
Sinks ($\text{mg H}_2\text{O}_2 \text{ m}^{-2} \text{ yr}^{-1}$)	$\text{H}_2\text{O}_2 + \text{OH}$	487.2	(28.1%)	19.0	(9.7%)	957.7	(35.0%)
	Photodissociation	534.7	(30.8%)	51.6	(26.5%)	893.7	(32.6%)
	Dry deposition	244.5	(14.1%)	31.8	(16.3%)	342.0	(12.5%)
	Wet deposition	410.8	(23.7%)	37.5	(19.2%)	255.2	(9.3%)
	Oxidation of SO_2	58.1	(3.3%)	55.1	(28.3%)	172.5	(6.3%)
Total		1735.3	(100.0%)	195.0	(100.0%)	2621.1	(95.8%)

^aFor Europe (defined as the box 20°W–40°E, 30°N–80°N), the budget is not balanced because of a net import or export term.

studies, but reaches 33.5% in our model. Oxidation of SO_2 by O_3 occurs principally during winter in the polluted regions, for example, over Europe, where the model overestimates cloud cover and precipitation. There is a coupling of the sulphate source from in-cloud oxidation, with the sink from wet scavenging. This would result in a lower net sulphate concentration in-cloud and consequently larger pH, at which the O_3 oxidation rate is enhanced leading to a predominance of this pathway.

The lifetimes for DMS, SO_2 , and sulfate are 1.1, 1.2, and 5.5 days, respectively. The lifetimes for DMS and SO_2 are slightly less than in previous studies, while the lifetime for sulfate is slightly greater than in previous studies (Chin et al., 2000a).

8 Sensitivity to Aqueous-Phase Chemistry

In some models, the oxidation of aqueous SO_2 by H_2O_2 is considered either as a titration of SO_2 with H_2O_2 or with a complete module of aqueous chemistry. In several of these models, H_2O_2 is replenished (i.e., it is regenerated to its prescribed value) at the beginning of each time step: every 40 minutes in Feichter et al. (1996), 4 hours in Chin et al. (1996), 3 hours in Chin et al. (2000a, 2000b), or 2

hours in Takemura et al. (2000). It is likely that such parameterizations overestimate the rate of oxidation of SO_2 by H_2O_2 as it can take a much longer time for H_2O_2 to replenish (see below).

In contrast, H_2O_2 is a prognostic species in the GISS GCM (Koch et al., 1999), in the NCAR CCM3 (Barth et al., 2000), and in the present study. The wintertime sulfate concentrations are underestimated in all three models, but to an even greater extent in the NCAR model, although it also considers oxidation of aqueous SO_2 by O_3 , while the GISS model does not. As shown in section 4.2, wintertime sulfate concentrations are also underestimated in our model. It is unlikely that this is due solely to a missing oxidation path for SO_2 , as SO_2 concentrations are also underestimated. Instead, this may be due to a too large precipitation rate over Europe in winter. It is, however, difficult to anticipate the extent to which the results would be improved if a more realistic precipitation field was simulated by the GCM. A smaller precipitation rate would increase the sulfate concentration, which would slow down the oxidation of SO_2 by O_3 , through a decrease in the cloud droplet pH. It appears that oxidation of SO_2 by O_3 is the major source of sulfates during winter in our model (Fig. 24). It is therefore likely that not only the oxidation rate of aqueous SO_2 , but also the scavenging rate of sulfate or the transport outside the boundary layer

are at stake. Moreover, it could be that the frequency of occurrence of precipitation is as important as the average precipitation rate to predict accurately the scavenging rate of sulfate (V. Ramaswamy, personal communication). However this parameter is usually not evaluated in GCMs and data are not readily available.

Another source of uncertainty stems from the computation of the pH of cloud droplets in our model. As evident from Eq. 1, one needs to know the concentration in ammonium cation to compute the pH. Our parametrization may not always be appropriate.

We made a sensitivity experiment where H_2O_2 is not depleted when it oxidizes SO_2 in the aqueous phase (NODEPL experiment). Therefore, in this run, H_2O_2 is not interactive with the sulfur cycle, but concentrations of SO_2 and sulfate still depend on H_2O_2 concentrations. Fig. 25a shows the surface mixing ratio of H_2O_2 in January in this sensitivity run. Mixing ratios are larger than in the base run by up to 200% over Europe in January (Fig. 25b). This difference between the two runs is corroborated by analyzing the budget of H_2O_2 in our base run. The concentration of H_2O_2 results from a balance between production from the HO_2+HO_2 reaction and sinks from photodissociation, dry and wet scavenging, and the reaction with OH. Our model does not include neither in-cloud production of H_2O_2 (Mc Elroy, 1986), nor does it include production of HO_x (OH and HO_2) and H_2O_2 from ozonolysis reactions of alkenes (Ariya et al., 2000). Globally- and annually-averaged, oxidation of SO_2 is a rather small sink for H_2O_2 , at about 3%. However on the regional scale this reaction can cause a much larger sink for H_2O_2 (see Table 6). This is the case over Europe in wintertime where oxidation of SO_2 represents 28% of the removal rate for H_2O_2 . The rather long lifetime of H_2O_2 in wintertime (around 2.5 days) and the importance of oxidation of SO_2 as a sink clearly indicate that the concentration of H_2O_2 cannot be held fixed in global sulfur models, as done in some of the previous studies.

9 Conclusion

We have incorporated the sulfur cycle in the general circulation model LMD-ZT and we have parameterized the processes of convective transport, wet scavenging, and aqueous-phase chemistry as consistently as possible with the model physical parameterizations. The model predicts the atmospheric fate of hydrogen peroxide (H_2O_2) and six sulfur species.

Comparison of surface modelled and observed sulfur distributions at remote monitoring stations shows a fair agreement except for MSA, whose production in the model should be reevaluated. We reiterate the finding previously made that surface concentrations of sulfates are underestimated during wintertime over Europe. We suspect that this is due to biases in the GCM climatology of cloud cover and precipitation, although this may also be due to too low oxidant levels during winter. The budget and concentra-

tion of H_2O_2 in Europe and the Northeast United States depend critically on the inclusion of the H_2O_2 sink associated to oxidation of SO_2 . We suggest that more effort should be made to measure and monitor the concentrations of hydrogen peroxide over polluted regions, and to assess quantitatively the sources and sinks of this species.

It also appears that, in a few cases, sulfate mixing ratios are overpredicted in the upper troposphere when compared with measurements made during the PEM campaigns. For the other species (DMS, SO_2 , and H_2O_2), the modelled vertical profile were generally in agreement, sometimes in disagreement with the PEM measurements, but there is no evidence for any systematic bias in the model.

While some improvements are still needed, we feel that this model is now a useful tool to investigate issues related to heterogeneous chemistry and to the climatic effects of natural DMS emissions and anthropogenic sulfate. In the near future we also plan to run our model in nudged mode and perform further evaluation against observations from field campaigns.

Acknowledgments : we are grateful to D. Hauglustaine, Y. Balkanski, E. Cosme, M. Lawrence, D. L. Roberts and M. C. Barth for helpful discussion, J. Sciare for providing the DMS data at Amsterdam Island, A. Hjellbrekke for providing the EMEP data, and R. Vet and C.-U. Ro for providing the EMEFS data.. The EMEFS data utilized in this study were collected and prepared under the co-sponsorship of the United States Environmental Protection Agency, the Atmospheric Environment Service, Canada, the Ontario Ministry of Environment, the Electric Power Research Institute, and the Florida Electric Power Coordinating Group. Olivier Boucher would like to thank P. Crutzen, J. Lelieveld, and the Max Planck Institute for Chemistry for their hospitality. Computer time for this study was provided by the Institut du Développement et des Ressources en Informatique Scientifique (IDRIS). This research project is supported by the Programme National de Chimie Atmosphérique (PNCA) of the CNRS and the Indo-French Centre for the Promotion of Advanced Research (IFCPAR).

References

- Aas, W., Hjellbrekke, A.-G., Semb, A., Schaug, J. 1999. Data Quality 1997, Quality Assurance, and Field Comparison, EMEP/CCC-Report6/99, 157 pp., Norsk institutt for luftforskning.
- Adams, P.J., Seinfeld, J.H., Koch, D.M., 1999. Global concentrations of tropospheric sulfate, nitrate, and ammonium aerosol simulated in a general circulation model. *Journal of Geophysical Research* 104, 13791–13823.
- Andreae, M.O., Elbert, W., Cai, Y., Andreae, T.C., Gras, J., 1999. Non-sea-salt sulfate, methanesulfonate, and nitrate aerosol concentrations and size distributions at Cape Grim, Tasmania. *Journal of Geophysical Research* 104, 21695–21706.

- Andres, R.J., Kasgnoc, A.D., 1998. A time-averaged inventory of subaerial volcanic sulfur emissions. *Journal of Geophysical Research* 103, 25251–25261.
- Ariya, P.A., Sander, R., Crutzen, P.J., 2000. Significance of HO_x and peroxides production due to alkene ozonolysis during fall and winter: A modelling study. *Journal of Geophysical Research* 105, 17721–17738.
- Atkinson, R., Baulch, D.L., Cox, R.A., Hampson, R.F., Kerre Jr., J.A., Troe, J., 1989. Evaluated kinetic and photochemical data for atmospheric chemistry: Supplement III. *Journal of Physical and Chemical Reference Data* 18, 881–1097.
- Ayers, G.P., Ivey, J.P., Gillett, R.W., 1991. Coherence between seasonal cycles of dimethyl sulphide, methanesulphonate and sulphate in marine air. *Nature* 349, 404–406.
- Ayers, G.P., Penkett, S.A., Gillett, R.W., Bandy, B., Galbally, I.E., Meyer, C.P., Elsworth, C.M., Bentley, S.T., Forgan, B.W., 1996. The annual cycle of peroxides and ozone in marine air at Cape Grim, Tasmania. *Journal of Atmospheric Chemistry* 23, 221–252.
- Balkanski, Y.J., D.J. Jacob, G.M. Gardner, W.C. Graustein, K.K. Turekian, 1993. Transport and residence times of tropospheric aerosols inferred from a global three-dimensional simulation of ^{201}Pb . *Journal of Geophysical Research* 98, 20573–20586.
- Barth, M.C., Hegg, D.A., Hobbs, P.V., 1989. Measurements of atmospheric gas-phase and aqueous-phase hydrogen peroxide concentrations in winter on the east coast of the United States. *Tellus* 41B, 61–69.
- Barth, M.C., Rasch, P.J., Kiehl, J.T., Benkovitz, C.M., Schwartz, S.E., 2000. Sulfur chemistry in the National Center for Atmospheric Research Community Climate Model: Description, evaluation, features, and sensitivity to aqueous chemistry. *Journal of Geophysical Research* 105, 1387–1415.
- Benkovitz, C.M., Berkowitz, C.M., Easter, R.C., Nemesure, S., Wagener, R., Schwartz, S.E., 1994. Sulfate over the North Atlantic and adjacent continental regions: Evaluation for October and November 1986 using a three-dimensional model driven by observation-derived meteorology. *Journal of Geophysical Research* 99, 20725–20756.
- Benkovitz, C.M., Scholtz, M.T., Pacyna, J., Tarrasón, L., Dignon, J., Voldner, E.C., Spiro, P.A., Logan, J.A., Graedel, T.E., 1996. Global gridded inventories of anthropogenic emissions of sulfur and nitrogen. *Journal of Geophysical Research* 101, 29239–29253.
- Boatman, J.F., Wellman, D.L., Van Valin, C.C., Gunter, R.L., Ray, J.D., Sievering, H., Kim, Y., Wilkison, S.W., Luria, M., 1989. Airborne sampling of selected trace chemicals above the central United States. *Journal of Geophysical Research* 94, 5081–5093.
- Boucher, O., Anderson, T.L., 1995. GCM assessment of the sensitivity of direct climate forcing by anthropogenic sulfate aerosols to aerosol size and chemistry. *Journal of Geophysical Research* 100, 26117–26134.
- Boucher, O., Lohmann, U., 1995. The sulfate-CCN-cloud albedo effect: a sensitivity study using two general circulation models. *Tellus* 47B, 281–300.
- Boucher, O., Moulin, C., Belviso, S., Aumont, O., Bopp, L., Cosme, E., von Kuhlmann, R., Lawrence, M.G., Pham, M., Reddy, M. S., Sciare, J., Venkataraman, C., 2002. Sensitivity study of DMS atmospheric concentrations and sulphate aerosols indirect radiative forcing to the DMS source representation and oxidation, submitted to *Atmospheric Chemistry and Physics*.
- Charlson, R.J., Schwartz, S.E., Hales, J.M., Cess, R.D., Coakley Jr., J.A., Hansen, J.E., Hofmann, D.J., 1992. Climate forcing by anthropogenic aerosols. *Science* 255, 423–430.
- Chatfield, R.B., Crutzen, P.J., 1990. Are there interactions of iodine and sulfur species in marine air photochemistry? *Journal of Geophysical Research* 95, 22319–22341.
- Chin, M., Jacob, D.J., Gardner, G.M., Foreman-Fowler, M.S., Spiro, P.A., 1996. A global three-dimensional model of tropospheric sulfate. *Journal of Geophysical Research* 101, 18667–18690.
- Chin, M., Rood, R.B., Lin, S.-J., Müller, J.-F., Thompson, A.M., 2000a. Atmospheric sulfur cycle simulated in the global model GOCART: model description and global properties. *Journal of Geophysical Research* 105, 24671–24688.
- Chin, M., Savoie, D.L., Huebert, B.J., Bandy, A.R., Thornton, D.C., Bates, T.S., Quinn, P.K., Saltzman, E.S., De Bruyn, W.J., 2000b. Atmospheric sulfur cycle simulated in the global model GOCART: comparison with field observations and regional budgets. *Journal of Geophysical Research* 105, 24689–24712.
- Chuang, C.C., Penner, J.E., Taylor, K.E., Grossman, A.S., Walton, J.J., 1997. An assessment of the radiative effects of anthropogenic sulfate. *Journal of Geophysical Research* 102, 3761–3778.
- Chuang, C.C., Penner, J.E., Prospero, J.M., Grant, K.E., Rau, G.H., 2002. Effects of anthropogenic aerosols on cloud susceptibility: A sensitivity study of radiative forcing to aerosol characteristics and global concentration. *Journal of Geophysical Research*, in press.

- Clarke, J.F., Edgerton, E.S., Martin, B.E., 1997. Dry deposition calculations for the clean air status and trends network. *Atmospheric Environment* 31, 3667–3678.
- Cosme, E., Genthon, C., Martinerie, P., Pham, M., Boucher, O., 2002. Sulfur cycle in the high southern latitudes in the LMD-ZT general circulation model. *Journal of Geophysical Research*, in press.
- Covert, D.S., 1988. North Pacific marine background aerosol: average ammonium to sulfate molar ratio equals 1. *Journal of Geophysical Research* 93, 8455–8458.
- Crutzen, P.J., Lawrence, M.G., 2000. The impact of precipitation scavenging on the transport of trace gases: a 3-dimensional model sensitivity study. *Journal of Atmospheric Chemistry* 37, 81–112.
- Dentener, F.J., Crutzen, P.J., 1993. Reaction of N_2O_5 on tropospheric aerosols: impact on the global distributions of NO_x , O_3 and OH. *Journal of Geophysical Research* 98, 7149–7163.
- Dentener, F., Williams, J., Metzger, S., 2002. Aqueous phase reactions of HNO_4 : the impact on tropospheric chemistry. *Journal of Atmospheric Chemistry* 41, 109–134.
- DeMore, W.B., Sander, S.P., Golden, D.M., Hampson, R.F., Kurylo, M.J., Howard, C.J., Ravishankara, A.R., Kolb, C.E., Molina, M.J., 1997. Chemical kinetics and photochemical data for use in stratospheric modeling. Evaluation Number 12, JPL Publication 97-4, Jet Propulsion Lab., Pasadena, CA.
- Feichter, J., Kjellström, E., Rodhe, H., Dentener, F., Lelieveld, J., Roelofs, G.-J., 1996. Simulation of the tropospheric sulfur cycle in a global climate model. *Atmospheric Environment* 30, 1693–1707.
- Garland, J.A., 1977. The dry deposition of sulphur dioxide to land and water surfaces. *Proceedings of the Royal Society of London A* 354, 245–268.
- Giorgi, F., Chameides, W.L., 1986. Rainout lifetimes of highly soluble aerosols and gases as inferred from simulations with a general circulation model. *Journal of Geophysical Research* 91, 14367–14376.
- Grossmann, D., 1999. Die Gasphaseozonolyse von Alkenen in Gegenwart von Wasserdampf als Quelle für Wasserstoffperoxid und organische Peroxide in der Atmosphäre. Ph. D. Thesis, University of Mainz.
- Heikes, B.G., Kok, G.L., Walega, J.G., Lazrus, A.L., 1987. H_2O_2 , O_3 and SO_2 measurements in the lower troposphere over the Eastern United States during fall. *Journal of Geophysical Research* 92, 915–931.
- Hoffmann, M.R., Calvert, J.G., 1985. Chemical transformation modules for Eulerian acid deposition models, Volume 2, The aqueous phase chemistry. EPA/600/3-85/017, US Environmental Protection Agency, Research Triangle Park, North Carolina, USA.
- Hourdin, F., Armangaud, A., 1999. The use of finite-volume methods for atmospheric advection of trace species. Part I: Test of various formulations in a general circulation model. *Monthly Weather Review* 127, 822–837.
- Hourdin, F., Issartel, J.-P., 2000. Sub-surface nuclear tests monitoring through the CTBT xenon network. *Geophysical Research Letters* 27, 2245–2248.
- Kasibhatla, P., Chameides, W.L., John, J.S., 1997. A three-dimensional global model investigation of seasonal variations in the atmospheric burden of anthropogenic sulfate aerosols. *Journal of Geophysical Research* 102, 3737–3760.
- Kettle, A.J., et al., 1999. A global database of sea surface dimethylsulfide (DMS) measurements and a procedure to predict sea surface DMS as a function of latitude, longitude, and month. *Global Biogeochemical Cycles* 13, 399–444.
- Koch, D., Jacob, D., Tegen, I., Rind, D., Chin, M., 1999. Tropospheric sulfur simulation and sulfate direct radiative forcing in the Goddard Institute for Space Studies general circulation model. *Journal of Geophysical Research* 104, 23799–23822.
- Langner, J., Rodhe, H., 1991. A global three-dimensional model of the tropospheric sulfur cycle. *Journal of Atmospheric Chemistry* 13, 225–263.
- Lee, M., Heikes, B.G., O’Sullivan, D.W., 2000. Hydrogen peroxide and organic hydroperoxide in the troposphere: a review. *Atmospheric Environment* 34, 3475–3494.
- Legates, D.R., Willmott, C.J., 1990. Mean seasonal and spatial variability in gauge-corrected, global precipitation, *International Journal of Climatology*, 10, 111–127.
- Lide, D.R., Frederikse, H.P.R., editors, 1995. *CRC Handbook of Chemistry and Physics*, 76th edition, CRC Press, Inc., Boca Raton, FL.
- Liss, P.S., Merlivat, L., 1986. Air-sea exchange rates: Introduction and synthesis, in *The Role of Air-Sea Exchange in Geochemical Cycling*, P. Buat-Ménard (Ed.), Norwell, Mass.
- Mari, C., Jacob, D.J., Bechtold, P., 2000. Transport and scavenging of soluble gases in a deep convective cloud. *Journal of Geophysical Research* 105, 22255–22267.
- Mc Elroy, W.J., 1986. Sources of hydrogen peroxide in cloudwater. *Atmospheric Environment* 20, 427–438.

- McNaughton, D.J., Vet, R.J., 1996. Eulerian model evaluation field study (EMEFS): A summary of surface network measurements and data quality. *Atmospheric Environment* 30, 227–238.
- Müller, J.-F., Brasseur, G.P., 1995. IMAGES: A three-dimensional chemical transport model of the global troposphere. *Journal of Geophysical Research* 100, 16455–16490.
- National Bureau of Standards, 1965. Selected values of chemical thermodynamic properties, 1. Tech. Note, 270–1, Gaithersburg, MD.
- O'Sullivan, D.W., Lee, M., Noone, B.C., Heikes, B.G., 1996. Henry's law constant determinations for hydrogen peroxide, methyl hydroperoxide, hydroxymethyl hydroperoxide, ethyl hydroperoxide, and peroxyacetic acid. *Journal of Physical Chemistry* 100, 3241–3247.
- Pham, M., Müller, J.-F., Brasseur, G., Granier, C., Mégie, G., 1995a. A three-dimensional study of the tropospheric sulfur cycle. *Journal of Geophysical Research* 100, 26061–26092.
- Pham, M., Müller, J.-F., Brasseur, G., Granier, C., Mégie, G., 1995b. A 3D model study of the global sulphur cycle: Contributions of anthropogenic and biogenic sources. *Atmospheric Environment* 30, 1815–1822.
- Pruppacher, H.R., Klett, J.D., 1997. *Microphysics of Clouds and Precipitation*, Second Revised and Enlarged Edition with an Introduction to Cloud Chemistry and Cloud Electricity, Kluwer Academic Publishers, Boston, 954 pp.
- Putaud, J.-P., Mihalopoulos, N., Nguyen, B.C., Campin, J.M., Belviso, S., 1992. Seasonal variations of atmospheric sulfur dioxide and dimethylsulfide concentrations at Amsterdam Island in the Southern Indian Ocean. *Journal of Atmospheric Chemistry* 15, 117–131.
- Rasch, P.J., Barth, M.C., Kiehl, J.T., Schwartz, S.E., Benkovitz, C.M., 2000. A description of the global sulfur cycle and its controlling processes in the National Center for Atmospheric Research Community Climate Model, Version 3. *Journal of Geophysical Research* 105, 1367–1385.
- Rodhe, H., 1999. Human impact on the atmospheric sulfur balance. *Tellus* 51AB, 110–122.
- Roelofs, G.-J., Lelieveld, J., Ganzeveld, L., 1998. Simulation of global sulfate distribution and the influence on effective cloud drop radii with a coupled photochemistry-sulfur cycle model. *Tellus* 50B, 224–242.
- Sakugawa, H., Kaplan, I.R., 1989. H_2O_2 and O_3 in the atmosphere of Los Angeles and its vicinity: factors controlling their formation and their role as oxidant of SO_2 . *Journal of Geophysical Research* 94, 12957–12973.
- Sander, R., 1999. *Compilation of Henry's Law Constants for Inorganic and Organic Species of Potential Importance in Environmental Chemistry (Version 3)*. Available at <http://www.mpch-mainz.mpg.de/~sander/res/henry.html>.
- Sciare, J., Baboukas, E., Hancy, R., Mihalopoulos, N., Nguyen, B.C., 1998. Seasonal variation of dimethylsulfoxide in rainwater at Amsterdam Island in the Southern Indian Ocean: implications on the biogenic sulfur cycle. *Journal of Atmospheric Chemistry* 30, 229–240.
- Sciare, J., Mihalopoulos, N., Dentener, F.J., 2000. Interannual variability of atmospheric dimethylsulfide in the southern Indian Ocean. *Journal of Geophysical Research* 105, 26,369–26,378.
- Seinfeld, J.H., Pandis, S.N., 1998. *Atmospheric Chemistry and Physics, From Air Pollution to Climate Change*. John Wiley & Sons, 1326 pp.
- Takemura, T., Okamoto, H., Maruyama, Y., Numaguti, A., Higurashi, A., Nakajima, T., 2000. Global three-dimensional simulation of aerosol optical thickness distribution of various origins. *Journal of Geophysical Research*, 105, 17853–17873.
- Thornton, D.C., Bandy, A.R., Blomquist, B.W., Davis, D.D., Talbot, R.W., 1996. Sulfur dioxide as a source of condensation nuclei in the upper troposphere of the Pacific Ocean. *Journal of Geophysical Research* 101, 1883–1890.
- Tiedtke, M., 1989. A comprehensive mass flux scheme for cumulus parameterization in large-scale models. *Quarterly Journal of the Royal Meteorological Society* 117, 1779–1800.
- van Leer, B., 1977. Towards the ultimate conservative difference scheme: IV. A new approach to numerical convection. *Journal of Computational Physics* 23, 276–299.
- Van Valin, C.C., Ray, J.D., Boatman, J.F., Gunter, R.L., 1987. Hydrogen peroxide in air during winter over the South-Central United States. *Geophysical Research Letters* 14, 1146–1149.
- Venkataraman, C., Mehra, A., Mhaskar, P., 2001. Mechanisms of sulphate aerosol production in clouds: effect of cloud characteristics and season in the Indian region. *Tellus* 53B, 260–272.
- Warneck, P., 1999. The relative importance of various pathways for the oxidation of sulfur dioxide and nitrogen dioxide in sunlit continental fair weather clouds. *Physical Chemistry and Chemical Physics* 1, 5471–5483.

- Watts, S.F., 2000. The mass budgets of carbonyl sulfide, dimethyl sulfide, carbon disulfide and hydrogen sulfide. *Atmospheric Environment* 34, 761-779.
- Wesely, M.L., Cook, D.R., Hart, R.L., Speer, R.E., 1985. Measurements and parameterization of particulate sulphur dry deposition over grass. *Journal of Geophysical Research* 90, 2131-2143.

Déjà paru :

- 11 : Décembre 1998** Gurvan Madec, Pascale Delecluse, Maurice Imbard and Claire Lévy, *OPA8.1 ocean general circulation model reference manual*.
- 12 : Janvier 1999** Marc Guyon, Gurvan Madec, François-Xavier Roux, Christophe Herbaut, Maurice Imbard, and Philippe Fraunie, *Domain Decomposition Method as a Nutshell for Massively Parallel Ocean Modelling with the OPA Model*.
- 13 : Février 1999** Eric Guilyardi, Gurvan Madec, and Laurent Terray, *he Role of Lateral Ocean Physics in the Upper Ocean Thermal Balance of a Coupled Ocean-Atmosphere GCM*
- 14 : Mars 1999** D. Hauglustaine, *Impact of Biomass Burning and Lightning Emissions on the Distribution of Tropospheric Ozone and its Precursors in the Tropics*
- 15 : Décembre 1999** L. Menut, R. Vautard, C. Honnoré, and M. Beekmann, *Sensitivity of Photochemical Pollution using the Adjoint of a Simplified Chemistry-Transport Model*
- 16 : Janvier 2000** J.-Ph. Boulanger, *The Trident Pacific model. Part 1: The oceanic dynamical model and observations during the TOPEX/POSEIDON period*
- 17 : Janvier 2000** J.-Ph. Boulanger and Christophe Menkes, *The Trident Pacific model Part 2: The thermodynamical model and the role of long equatorial wave reflection during the TOPEX/POSEIDON period*
- 18 : Octobre 2000** H. Le Treut and B. McAvaney, *A model intercomparison of equilibrium climate change in response to CO₂ doubling*
- 19 : Octobre 2000** Pierre Friedlingstein, Laurent Bopp, Philippe Ciais, Jean-Louis Dufresne, Laurent Fairhead, Hervé LeTreut, Patrick Monfray, and James Orr, *Positive feedback of the carbon cycle on future climate change*
- 20 : Février 2001** Agnès Ducharne, Catherine Golaz, Etienne Leblois, Katia Laval, Emmanuel Ledoux, and Ghislain de Marsily, *RiTHM (River Transfer Hydrological Model) : a Runoff Routing Scheme for GCMs*
- 21 : Octobre 2001** Y. Le Clainche, P. Braconnot, O. Marti, S. Joussaume, J-L. Dufresne, and M-A. Filiberti, *The role of sea ice thermodynamics in the Northern Hemisphere climate as simulated by a global coupled ocean-atmosphere model*
- 22 : Janvier 2002** P. de Rosnay, *A GCM experiment on time sampling for remote sensing of near-surface soil moisture*
- 23 : Juillet 2002** O. Boucher, M. Pham, C. Venkataraman, *Simulation of the atmospheric sulfur cycle in the Laboratoire de Météorologie Dynamique General Circulation Model. Model Description, Model Evaluation, and Global and European Budgets*